Calhoun
Institutional Archive of the Naval Postgraduate School

**Calhoun: The NPS Institutional Archive**

**DSpace Repository**

Theses and Dissertations | 1. Thesis and Dissertation Collection, all items

1997-09

# Microstructure, composition and crystallography of Aalbrog Lion Brand Danish White cement

Maldonado, Fernando.

Monterey, California. Naval Postgraduate School

http://hdl.handle.net/10945/26632

This publication is a work of the U.S. Government as defined in Title 17, United States Code, Section 101. Copyright protection is not available for this work in the United States.

*Downloaded from NPS Archive: Calhoun*

http://www.nps.edu/library

Calhoun is the Naval Postgraduate School's public access digital repository for research materials and institutional publications created by the NPS community. Calhoun is named for Professor of Mathematics Guy K. Calhoun, NPS's first appointed -- and published -- scholarly author.

Dudley Knox Library / Naval Postgraduate School
411 Dyer Road / 1 University Circle
Monterey, California USA 93943

NPS ARCHIVE
1997.09
MALDONADO, F.

# NAVAL POSTGRADUATE SCHOOL
# MONTEREY, CALIFORNIA

# THESIS

**MICROSTRUCTURE, COMPOSITION AND CRYSTALLOGRAPHY OF AALBROG LION BRAND DANISH WHITE CEMENT**

by

**Fernando Maldonado**

**September, 1997**

**Thesis Advisor:** **Alan G. Fox**

Thesis
M2178135

**Approved for public release; distribution is unlimited.**

DUDLEY KNOX LIBRARY
NAVAL POSTGRADUATE SCHOOL
MONTEREY CA 93943-5101

# REPORT DOCUMENTATION PAGE

Form Approved OMB No. 0704-0188

Public reporting burden for this collection of information is estimated to average 1 hour per response, including the time for reviewing instruction, searching existing data sources, gathering and maintaining the data needed, and completing and reviewing the collection of information. Send comments regarding this burden estimate or any other aspect of this collection of information, including suggestions for reducing this burden, to Washington Headquarters Services, Directorate for Information Operations and Reports, 1215 Jefferson Davis Highway, Suite 1204, Arlington, VA 22202-4302, and to the Office of Management and Budget, Paperwork Reduction Project (0704-0188) Washington DC 20503.

| 1. AGENCY USE ONLY *(Leave blank)* | 2. REPORT DATE<br>September 1997 | 3. REPORT TYPE AND DATES COVERED<br>Master's Thesis |
|---|---|---|

4. TITLE AND SUBTITLE MICROSTRUCTURE, COMPOSITION AND CRYSTALLOGRAPHY OF AALBROG LION BRAND DANISH WHITE CEMENT

5. FUNDING NUMBERS

6. AUTHOR(S) Fernando Maldonado

7. PERFORMING ORGANIZATION NAME(S) AND ADDRESS(ES)
Naval Postgraduate School
Monterey CA 93943-5000

8. PERFORMING ORGANIZATION REPORT NUMBER

9. SPONSORING/MONITORING AGENCY NAME(S) AND ADDRESS(ES)

10. SPONSORING/MONITORING AGENCY REPORT NUMBER

11. SUPPLEMENTARY NOTES The views expressed in this thesis are those of the author and do not reflect the official policy or position of the Department of Defense or the U.S. Government.

12a. DISTRIBUTION/AVAILABILITY STATEMENT
Approved for public release; distribution is unlimited.

12b. DISTRIBUTION CODE

13. ABSTRACT *(maximum 200 words)* The morphology and crystallography of fully hardened Aalbrog Lion Brand Danish White cement paste (water-to-cement ratio 0.25) were examined using x-ray diffraction, optical and scanning electron microscopy with energy dispersive x-ray analysis (EDX) and transmission electron microscopy and EDX. These experiments showed the hardened cement to be mostly comprised of equiaxed particles of $3CaO.SiO_2$ with diameter of the order of 10 μm and larger often surrounded by inner and outer regions of an amorphous gel-like matrix with an average composition of about $1.75CaO.SiO_2.3H_2O$ (C-S-H) in which the $CaO/SiO_2$ ratio varied from about $0.35 \rightarrow 5.74$. The hydrated regions were also found to contain significant amounts of $Ca(OH)_2$. Small amounts of ettringite ($Ca_6Al_2(SO_4,SiO_4,CO_3)_3(OH)_{12}.26H_2O$) were also detected. In addition, selected area electron diffraction of the C-S-H matrix revealed diffuse rings, indicating the presence of short range ordering. The morphology of C-S-H matrix was found to be comprised of small 'cells' of size approximately 5 nm which are no doubt responsible for the good mechanical properties of this particular hardened cement paste. These results were also found to be in excellent agreement with previous research on this topic.

14. SUBJECT TERMS Calcium Silicate Hydrate (C-S-H), Portland cement, Short range ordering, Portlandite, ettringite.

15. NUMBER OF PAGES 84

16. PRICE CODE

| 17. SECURITY CLASSIFICATION OF REPORT | 18. SECURITY CLASSIFICATION OF THIS PAGE | 19. SECURITY CLASSIFICATION OF ABSTRACT | 20. LIMITATION OF ABSTRACT |
|---|---|---|---|
| Unclassified | Unclassified | Unclassified | UL |

NSN 7540-01-280-5500

Standard Form 298 (Rev. 2-89)
Prescribed by ANSI Std. 239-18 298-102

**Approved for public release; distribution is unlimited.**

# MICROSTRUCTURE, COMPOSITION AND CRYSTALLOGRAPHY OF AALBROG LION BRAND DANISH WHITE CEMENT

Fernando Maldonado
Lieutenant, United States Navy
B.S., University of Puerto Rico, 1985

Submitted in partial fulfillment
of the requirements for the degree of

**MASTER OF SCIENCE IN MECHANICAL ENGINEERING**

from the

**NAVAL POSTGRADUATE SCHOOL**
**September 1997**

NPS Archive
1997.09
Maldonado, F.

Thesis
M218135
c.2

DUDLEY KNOX LIBRARY
NAVAL POSTGRADUATE SCHOOL
MONTEREY CA 93943-5101

# ABSTRACT

The morphology and crystallography of fully hardened Aalbrog Lion Brand Danish White cement paste (water-to-cement ratio 0.25) were examined using x-ray diffraction, optical and scanning electron microscopy with energy dispersive x-ray analysis (EDX) and transmission electron microscopy and EDX. These experiments showed the hardened cement to be mostly comprised of equiaxed particles of $3CaO.SiO_2$ with diameter of the order of 10 μm and larger often surrounded by inner and outer hydrated regions of an amorphous gel-like matrix with an average composition of about $1.75CaO.SiO_2.3H_2O$ (C-S-H) in which the $CaO/SiO_2$ ratio varied from about $0.35 \rightarrow 5.74$. The hydrated regions were also found to contain significant amounts of $Ca(OH)_2$. Small amounts of ettringite ($Ca_6Al_2(SO_4,SiO_4,CO_3)_3(OH)_{12}.26H_2O$) were also detected. In addition, selected area electron diffraction of the C-S-H matrix revealed diffuse rings, indicating the presence of short-range ordering. The morphology of C-S-H matrix was found to be comprised of small 'cells' of size approximately 5 nm which are no doubt responsible for the good mechanical properties of this particular hardened cement paste. These results were also found to be in excellent agreement with previous research on this topic.

## TABLE OF CONTENTS

I. INTRODUCTION....1

II. BACKGROUND....5

A. BRIEF HISTORY OF CEMENT....5

B. PRODUCTION METHODS....6

C. THE CHEMISTRY OF CEMENT HYDRATION....7

1. Before hydration....7

2. After hydration....8

D. CEMENT CRYSTALLOGRAPHY AND MICROSTRUCTURE....10

E. MECHANICAL PROPERTIES....13

1. Brittle fracture....14

2. Stress-strain behavior....15

3. Mechanisms of plastic deformation....15

4. Influence of porosity....16

5. Hardness....17

F. DIFFICULTIES IN MICROSTRUCTURAL CHARACTERIZATION OF CEMENT....17

G. SCOPE OF PRESENT WORK....18

III. EXPERIMENTAL PROCEDURE....25

A. SAMPLE DESCRIPTION....25

B. SAMPLE PREPARATION....25

C. LOSS ON IGNITION....27

D. SCANNING ELECTRON MICROSCOPY....27

E. TRANSMISSION ELECTRON MICROSCOPY....28

F. OPTICAL MICROSCOPY....28

G. X-RAY DIFFRACTOMETRY....28

IV. RESULTS AND DISCUSSION....33

A. LOSS ON IGNITION....33

B. X-RAY DIFFRACTION....33

C. OPTICAL AND SCANNING ELECTRON MICROSCOPY (SEM)....35

D. TRANSMISSION ELECTRON MICROSCOPY....37

V. SUMMARY....65

A. CONCLUSIONS....65

B. RECOMMENDATIONS....66

LIST OF REFERENCES....69

INITIAL DISTRIBUTION LIST....73

## ACKNOWLEDGMENTS

I would like to express my sincere appreciation to my advisor Professor Alan G. Fox for his guidance, assistance and humor in helping me to complete this thesis on time.

Special acknowledgment is due to Dr. Martin Saunders and Dr. Sarath Menon for assistance and suggestions in the laboratory. Additionally, thanks are due to Richard Hashimoto for his valuable assistance and training.

I would like to dedicate this thesis to all my loved ones who have supported me during my time of study while at the Naval Postgraduate School. Specifically my Lord, parents, and sons Carlos and Xavier who understood the need for their father to spend so many nights and weekends away from them studying at school. A very special thanks to Deroline, my lovely and beautiful wife, whose love and encouragement were instrumental for me in my completion of this thesis and also in my Naval career.

# I. INTRODUCTION

Portland cement is the most common building material in use today. Over seventy million tons of cement are used in the United States every year. The characteristic feature of these materials is that when mixed with water, they form a paste that subsequently sets and hardens. This trait is especially useful in that solid and rigid structures having just about any shape may be expeditiously formed. The reaction products form a rigid, monolithic microstructure which has important binding and strength characteristics. While much is known about the chemistry of cement hydration , the physical details of the dilution and reprecipitation processes are not completely understood. Important questions about strength development, durability, and toughness can be addressed, not only by optical microscopy, but also by scanning electron microscopy (SEM), transmission electron microscopy (TEM), X-ray diffractometry (XRD) and neutron diffraction studies of the cement hydration. These techniques can assist in revealing the mechanisms of hydration.

An important application for cement is for shielding and waste disposal. Recently, the U.S. Government has begun research for an appropriate material that could be used to build storage sites for more than 33,000 tons of radioactive waste. The spent nuclear fuel, now at reactors in 41 states, will remain deadly for 10,000 or more years. The idea is to build a permanent underground repository for the waste, so once it is moved to this centralized site it will never be moved again. Currently, the waste in the form of used reactor fuel rods are maintained in water storage pools at reactor sites. However, these storage pools are either full already or filling up at a rate of 2,000 tons a year. Therefore,

the government needs storage sites able to accept waste as early as 2003. Cement has been proposed as the material to be use to build these sites or containers. The reasoning behind this is that cement, which is highly refractive, can absorb the highly penetrating neutrons from the spent nuclear fuel. Neutron shielding is best achieved by materials which have high absorption cross-section, particularly if there is a space limitation. Gamma-radiation, on the other hand, is best absorbed by dense materials of heavy atoms. Therefore, the surface of cement materials could be used to adsorb damaging radioactive fission products, such as $Cs^{127}$ and $Sr^{90}$.

Unfortunately, one of the main drawback to the use of cement, or any ceramic for that matter, is its disposition to brittle and catastrophic failure, due to its low fracture toughnesses. Therefore, until an effective type of cement with improved mechanical properties is designed for this use, the potential of this material will not be fully realized.

The purpose of this research program is: to investigate the microstructure and properties of Aalbrog Lion Brand Danish white cement, and to characterize the Calcium Silicate Hydrate (C-S-H gel)*, which is the main component of the hydration of Danish white cement. The reason it is important to investigate this particular brand is because it appears to have better toughness properties. Unfortunately, the structure of C-S-H is not well understood. C-S-H is believed to have a layered structure; but, a precise structural determination has not been performed because of lack of long-range crystallinity, as its structure appears to be nearly amorphous.

* The following cement chemical notation is used here: C is CaO, S is $SiO_2$, A is $Al_2O_3$, H is $H_2O$, F is $Fe_2O_3$, $\overline{S}$ is $SO_3$, etc.

The characterization of the C-S-H gel should help resolve the issue of possible sub crystalline regions, and local compositional order, which could be responsible for variations in mechanical properties in Portland cements.

In order to meet these research goals, the Australian Nuclear Science and Technology Organization (ANSTO), in conjunction with the Naval Postgraduate School (NPS) are actively investigating the morphology and microstructure of a reaction product of Danish white cement with a water to cement ratio of approximately 25 % (w/c=0.25). It is important to understand the morphology of the cement microstructure in order to determine the degree of improvement in the fracture toughness. A small angle neutron scattering (SANS) analysis of these materials on a nanometer scale suggests that the 'better' cements have equiaxed fine structures, rather than a needle-like morphology [1, 2]. Therefore, because Aalbrog Lion Brand Danish white cement appears to have improved mechanical properties, the focus of this study is to investigate it by optical microscopy, x-ray diffraction (XRD), scanning electron microscopy with energy dispersive x-ray analysis (SEM/EDX) and transmission electron microscopy (TEM) with EDX, to see if its improved mechanical properties can be understood from a microstructural point of view.

## II. BACKGROUND

### A. BRIEF HISTORY OF CEMENT

The use of cementitious substances for binding together fragments of stone is older than recorded history. However, the credit for demonstrating that a limestone containing clay, when burned and ground, possessed the property of hardening with water, is due to Mr. John Smeaton. This was in 1756, while he was searching for a suitable material to build the Eddystone Lighthouse [3]. In 1796 the manufacturing process was patented as the product of "Roman Cement". In 1824, Joseph Aspdin of Leeds, England, patented the process to manufacture 'Portland Cement'.

M. H. LeChatelier divided the hydraulic products of cements into several classes with one being Portland cement. He was the first to use the optical microscope to study cement clinker (the unhydrated material after firing) and was able to gain some knowledge of its constitution [4]. Using polarized light microscopy he discovered that tricalcium silicate was the principal constituent of cement clinker. The use of optical microscopy together with new technology allowed A. E. Tornebohm to discover the five principal constituents of cement clinker, which were found to be $3CaO.SiO_2$, $4CaO.Al_2O_3.Fe_2O_3$, birefringent calcium aluminate and some isotropic residues [4]. Then, in 1907, the first Code of Practice for reinforced concrete was published. Before this, there were many different cements on the market, more than matched by the number of client specifications. This agreement, of course was a major step in terms of design code, which had a strong emphasis on materials as well as on design calculations [5].

Since the original Code of Practice was published, cement standards have changed and developed in other ways. Still operating from a base of Portland cement clinker and calcium sulfate, there are a range of manufactured cements available, created by introducing additional major or minor constituents and additives. However, it is interesting to note that the dominating factor in the selection process has shifted to better durability (improved toughness), representing a substantial change in performance requirements.

Technological advancements such as x-ray diffraction, scanning electron microscopy and transmission electron microscopy, have been important tools for research into the crystallography and microstructure of cement clinker and its hydration products and have allowed an improved understanding of the material. However, because of the peculiarities in the constitution of Portland cement, the requirements for microscopy are very exacting. Although the constituents are non-metallic, most of them are so fine grained and highly refractive, that they are transparent only in thin grains. Additionally, the refractive indices of several constituents are very similar making characterization by optical microscopy very difficult. As a result materials scientists are trying to make use of x-ray and neutron diffraction and electron microscopy to try and understand the constitution of cement products.

## B. PRODUCTION METHODS

Portland cement is produced, in general, by grinding and mixing clay and lime-bearing minerals in the appropriate proportions for the cement concerned (see next sections), and then heating the mixture above 1400°C in a rotary kiln, so that physical and chemical

changes occur in the original material. The resulting product is called a 'clinker'. This 'clinker' then is ground into very fine powder to which is added a small amount of $CaSO_4.2H_2O$ (gypsum), which retards the setting process of the hydrated cement so that it hardens in a controlled manner. The overall product of this process is then called Portland cement. The properties of each type of Portland cement will vary depending to large degree on its composition.

## C. THE CHEMISTRY OF CEMENT HYDRATION

The chemistry of cement hydration is a very large subject, and of necessity only certain important areas of it will covered here. The idea is to deal with fundamental aspects rather than with details, even though a number of the latter are of immediate technical significance. The behavior on hydration of some of minor phases and components (e.g. iron-containing compounds) is therefore not considered. Attention has been centered on the proportions, structure, nature, and general mechanical properties of the various phases formed on hydration.

### 1. Before hydration

The typical phase composition for a regular cement (including the Aalbrog Lion Brand Danish White studied in the present work) is: 50 - 70 % alite, which is tricalcium silicate, $C_3S$ ($3CaO.SiO_2$, or $Ca_3SiO_5$). Others phases present are belite, which is dicalcium silicate ($C_2S$ or $2CaO.SiO_2$) 10 - 20 %, cubic tricalcium aluminate ($C_3A$ or $3CaO.Al_2O_3$) 3%, monoclinic tricalcium aluminate ($C_3A$) 1%, and the ferrite phase ($C_4AF$ or $4CaO.Al_2O_3.Fe_2O_3$ ) approx. 1%. There may also be a small amount of gypsum ($CaSO_4.2H_2O$) added. The alite composition of the Aalbrog Lion Brand Danish cement is

a little bit higher than normal Portland cements, but in general, the compositions are very similar [6, 7].

**2. After hydration**

Portland cement is the most common of the hydraulic cements; see Figure 2.1 for phase details. The hydration reaction, although complicated, is indicative of the general principles governing the hydration reactions of cements:

$$Ca_3Al_2O_6 + 6H_2O \leftrightarrow Ca_3Al_2(OH)_{12}\,, \tag{2.1}$$

$$2Ca_2SiO_4 + (5 - y + x)H_2O \leftrightarrow Ca_2[SiO_2(OH)_2]_2.(CaO)_{.y-1}.xH_2O + (3 - y)Ca(OH)_2\,, \tag{2.2}$$

$$2Ca_3SiO_5 + (5 + x)H_2O \leftrightarrow Ca_2[SiO_2(OH)_2]_2.(CaO).xH_2O + 3\ Ca(OH)_2\,, \tag{2.3}$$

In Eq. (2.2), $y$ is approximately 2.3. The value of $x$ in the hydrated calcium silicate (C-S-H) varies from zero to more than one, depending on the amount of water used. In each case the hydrated form of the cement is slightly less soluble than the anhydrous phases and as result, solution and precipitation occur through the liquid medium [7, 8].

The total constitution after hydration depends a great deal on the water/ cement ratio, with C-S-H as the principal reaction product of the clinker with water. C-S-H is typical of materials without highly ordered crystal structures. C-S-H has a variable composition that can be studied by x-ray diffraction and electron microscopy and these show that the C-S-H is in a somewhat colloidal gel form. C-S-H can form over a relatively wide range of Ca:Si ratios, indicating compositional and structural variability throughout this gel phase. Average Ca:Si ratios in hydrated cement paste have been determined previously by chemical analysis to range between 1.5 and 2.0 [9]. In agreement with this, electron microprobe analysis (EMPA) and SEM with energy dispersive X-ray analysis (EDX), with

their accurate and fully corrected chemical analyses of individual features, have yielded values between 1.6 and 1.9. In addition, early studies of ground and redispersed pastes, have revealed wide variabilities on a micrometer scale, demonstrating the presence of significant compositional heterogeneity throughout the gel phase.

Others phases are predicted but difficult to detect by SEM with EDX and XRD. When polished sections are used in SEM, the region analyzed is on the micrometer scale, which may be larger than the scale of compositional fluctuations. However, it can still be used, to compare the average composition between the several particles present. When the transmission electron microscope (TEM) is used, much smaller volumes can be analyzed; these can be as small as a few nanometers in each dimension if the sample is thinned sufficiently to reduce beam spreading effects [9, 10]. EMPA can be use to map the surface and provide spatial information in bulk specimens, but it can lead to misinterpretations in the analysis, due to the poor x-ray spatial resolution and the inability to resolve unseen surface inhomogeneities. In general, for thin specimens, the x-ray resolution in the TEM will be close to the size of the probe used. This allows the identification of features on a nanometer scale. The measuring (spatial resolution) range of various analytical instruments is shown in Figure 2.2. However, because the nature of the hydrated cement products, the preparation of thin samples for TEM analysis is very difficult [9] and they damage rapidly in the electron beam.

EDX analysis yields atomic ratios, which are adequate for determining local Ca:Si ratio fluctuations. As mentioned before, previous TEM/EDX investigations consistently

have revealed wide variabilities in the local Ca:Si ratio throughout the gel, which demonstrate the fluctuations at the nanometer scale [9].

Some of the additional phases that can be present after the hydration reaction are: unreacted $C_3S$, small amounts of unreacted $C_2S$, $Ca(OH)_2$ portlandite and small amounts of $Ca_6Al_2(SO_4.SiO_4.CO_3)_3(OH)_{12}.26H_2O$ ettringite [9, 10].

## D. CEMENT CRYSTALLOGRAPHY AND MICROSTRUCTURE

As mentioned above, hydrated calcium silicate (C-S-H) is the major reaction product of clinker with water. C-S-H makes up approximately 50-60% of the total volume, and forms the binding agent between the unreacted $C_3S$ and $C_2S$ and other crystalline phases. Unfortunately, the structure of C-S-H is not well understood, because it exhibits very low crystallinity [11]. To help with the understanding of the C-S-H structure, some similarities between the gel and tobermorite and jennite have previously been considered. Both jennite and tobermorite are believed to have layered structures that are stacked along the [001] direction, however, the crystal structure of either of these materials, has not been determined [9]. A general comparison of the C-S-H gel structure with either tobermorite or jennite reveal many similarities. In the past, both tobermorite and jennite models have been proposed as model to explain the structure of the C-S-H gel. However, the structural formula for jennite with an average Ca:Si ratio of 1.5 is $Ca_9(Si_6O_{18}H_2)(OH)_8.6H_2O$, and for tobermorite with an Ca:Si ratio of 0.83 it is $Ca_5(Si_6O_{18}H_2).8H_2O$. This suggests that, for these materials, some silicate tetrahedra may be missing. The structure of C-S-H differs from both of these crystalline substances,

mainly because C-S-H is nearly amorphous and it has a higher average Ca:Si ratio than jennite and tobermorite [9, 10].

It is the general belief that there are numerous types of C-S-H. However no compositional difference between them has been firmly proposed. Rather, it is possible that the morphology of C-S-H changes in response to different conditions of formation. Recent studies identified an inner and an outer region of the C-S-H phase that could be distinguished by significant morphological differences [9, 10, 12]. With no clear compositional difference between the two types of regions, the outer C-S-H forms on the surface of $C_3S$, as the hydration begins, whereas inner C-S-H is forms in the later stages of hydration as it proceeds into the $C_3S$ grains. Additionally, the coexistence of various other second phases within the C-S-H gel has been predicted. These include $Ca(OH)_2$ (CH); $(Ca_3(Al,Fe)(OH)_6.12H_2O)_2.X_3.xH_2O$ (Aft), where X is one formula unit of an oxide; $(Ca_2(Al,Fe)(OH)_6).X.xH_2O$ (Afm) [10].

The internal stress state in which the product is formed, has also been found to be responsible for some of the morphological differences. C-S-H formed near the surface under unconstrained boundary conditions is more structured, and porous, while the C-S-H formed below the surface of the particle, under highly constrained conditions, is more massive and structureless [9]. Thus the internal stress is believed to cause some of the morphological differences between the inner and outer products of the reaction. Some of these changes at the micron scale may occur during phase separation or formation.

Along with C-S-H, calcium hydroxide (CH) is formed as a by-product, which occurs as small hexagonal plates. The calcium hydroxide can react with carbon dioxide in the air or water available to form calcium carbonate. The chemical reaction of carbonation is:

$$Ca(OH)_2 + CO_2 \rightarrow CaCO_3 + H_2O \qquad (2.4)$$

This reaction will generate a lot of porosity within the C-S-H gel. As will be seen later, the porosity should be kept as low as possible if the optimum mechanical properties from the cement are to be obtained.

As mentioned before, in addition to the C-S-H and the C-H phases, other crystalline phases such as unhydrated $C_3S$, which can exist in several crystal polymorphs (rhombohedral, monoclinic, and triclinic) and unhydrated $C_2S$, which also has several polymorphs ($\alpha$, $\alpha'$, $\beta$, and $\gamma$) can also be present in the hydrated material. Hexagonal ettringite and monoclinic larnite can also be found. The two phases ($C_3S$ and $C_2S$) have similar XRD patterns with many overlapping lines, and the analysis of each is also complicated by variations in crystal structure. Ettringite can be detected, during the early stages of hydration, mainly because it generates low angle x-ray lines that at later stages, cannot easily be detected due to the high dense structure of the hardened paste. The amount, composition, and morphology of these minor phases will depend a great deal on the raw materials used, the conditions for sintering, hydration conditions and the water to cement ratio.

The bottom line is, different cements can have very different characteristics, but often the only difference between them chemically is just a small amount of different oxides such as: $3CaO.Al_2O_3$, $Fe_2O_3$ and $CaSO_4$ etc... and it is difficult to see any differences between

the various cements by XRD and SEM/EDX. However, it would seem that the morphology of the reaction products is very important and these cannot be seen very well optically or by SEM since they seem to vary on a nanometer scale. In terms of the morphology of the microstructure on a nanometer scale, it would appear that the 'better' (in terms of mechanical properties) cements have equiaxed fine structure, rather than needle-like [1].

## E. MECHANICAL PROPERTIES

The mechanical properties of cements as well as most ceramics are, in many respects, inferior to those of metals. The principal drawback is a disposition to catastrophic brittle fracture with little energy absorption.

The cement must first of all have cohesive strength. Probably equally important, the cement must adhere to the aggregate with the best cements being those whose products are not highly crystalline. The reasoning behind this is that an amorphous or finely colloidal cement is more likely to match the structure of the aggregate and develop good adhesion than a highly crystalline cement. In addition, an amorphous structure is somewhat flexible, so that it does not develop severe stress concentrations when loads or dimensional changes are encountered.

The ratio of water to cement in the mix has a primary effect on the final strength of the cement. As long as adequate water is added for hydration and for workability, the lower the water to cement ratio, the higher the resulting strength [13]. In addition, the behavior (e.g., brittle fracture, stress-strain, plastic deformation, etc...) depends on its composition. In other words, it depends on what phases are present and in what proportions. Thus a

knowledge of the proportion of each phase in cement or clinker should make it possible to predict the behavior of Portland cement and its reaction products. Some of the properties, in general, are described below:

**1. Brittle fracture**

At normal temperatures, cements almost always fracture before plastic deformation can occur in response to an applied tensile load. Crack growth in crystalline specimens is usually through the grains and along specific crystallographic (cleavage) planes of high atomic density. The measured fracture strengths are lower than the predicted by the theory from interatomic bonding forces. This is due to very small flaws present in the material which serve as stress raisers. These stress raisers may be minute surface or interior microcracks, internal pores, and grain corners, which are hard to control.

The measure of the material's ability to resist fracture when a crack is present is specified in terms of fracture toughness. Plane fracture toughness values for ceramic materials are much smaller than for metals; typically they are below 10 Mpa $(m)^{0.5}$ [6].

There is usually significant variation in the fracture strength for many specimens. A distribution of fracture strengths for Portland cement is shown in Figure 2.3. The phenomenon is explained by the dependence of the fracture strength on the probability of the existence of a flaw that is will initiate a crack. This probability varies from specimen to specimen for the same material and depends on fabrication technique, w/c ratio and variations in processing treatment. Specimen size or volume also influences the fracture strength; the larger the specimen, the greater the flaw existence probability and thus the likelihood of a lower fracture strength.

For compressive stresses, there is no stress amplification associated with any preexisting flaws. Therefore, cements display much higher strengths in compression than in tension, and they are generally utilized when load conditions are compressive. In addition, the fracture strength may be enhanced by imposing residual compressive stresses at the surface, particularly by thermal tempering.

**2. Stress-strain behavior**

The stress-strain behavior on brittle ceramics can be obtained generally by transverse bending test, in which a rod specimen having either a circular or rectangular cross section is bent until fracture using a three or four point loading technique; the three point loading scheme is illustrated in Figure 2.4. At the point of loading, the top surface of the specimen is placed in compression, while the bottom surface is in tension. The stress is computed from the specimen thickness, the bending moment, and the moment of inertia of the cross section; these parameters are noted in the Figure. The maximum stress at fracture using this test, is the modulus of rupture, or the bending strength.

The elastic stress-strain behavior obtained from these transverse bending tests is similar to the tensile tests for metals; i.e. there is a linear relationship between stress and strain.

**3. Mechanisms of plastic deformation**

At room temperature cement is expected to fracture before the onset of plastic deformation, however there is still a possibility that deformation may occur. The deformation is different for crystalline and noncrystalline components. For crystalline phases (e.g., in $C_3S$ and $C_2S$), plastic deformation occurs by the motion of dislocations. As a result, one reason for the brittleness of cementitious materials is the lack of slip

systems present, along which dislocations may move ($C_3S$ and $C_2S$ have complex crystal structures with few slip systems). For amorphous phases, which is the case of the C-S-H phase, deformation occurs by viscous flow in the same way that amorphous polymers deform; the rate of deformation is proportional to the applied stress. In response to an applied shear stress, atoms or ions slide past one another by the breaking and reforming of interatomic bonds.

**4. Influence of porosity**

Porosity has a negative influence on both the elastic properties and strength. It has been observed that the magnitude of the modulus of elasticity $E$ decreases with volume fraction porosity, $P$, according to:

$$E=E_0(1-1.9P+0.9P^2) \qquad (2.5)$$

where $E_0$ is the modulus of elasticity of the nonporous material. Porosity decreases the fracture strength because the pores reduce the cross sectional area across which the load is applied and because they act as stress concentrators. A 10 vol% porosity will decrease the modulus of rupture by 50% from measured value for the non-porous material [6].

Major progress has occurred in recent years in the manufacture of hydraulic cements of decreased porosity and increased strength. One method involves adding ultrafine $SiO_2$ ("microsilica") particles to the cement. The process is referred to as DSP (densified with small particles) cement. The $SiO_2$ particles are much smaller than the cement particles and will fill voids between the latter. In addition, less water is required to prepare a mix. The decreased water and better particle packing result in decreased total porosity and a large decrease in pore size. Strength can be increased by a factor of 4 and permeability to

liquid absorption nearly eliminated [14]. The life of road, bridge, and building structures, and in the present case the radioactive waste repositories can be greatly increased, especially those that contain metal reinforcing bars which are attacked in conventional concrete by corrosion.

A second method to improve hydraulic cements is called macro-defect free (MDF) cement. This approach utilizes organic additives to the cement to achieve better dispersion and particle packing. It also increases the strength and decreases the permeability with little increase in cost. Figure 2.5 illustrates some of the improvements that have occured in advanced cements in recent years [14].

### 5. Hardness

Hardness is one of the beneficial properties of ceramics in general, in fact, the hardest known materials are ceramics.

Generally, the properties of any concrete structure formed will depend heavily on the amount of porosity present, the strength of any aggregate material or reinforcement (e.g., crushed stone, steel bars), and the properties of the C-S-H phase.

## F. DIFFICULTIES IN MICROSTRUCTURAL CHARACTERIZATION OF CEMENT

Characterization of the cement microstructure is very important because it helps to establish the proper conditions for manufacture (e.g., texture of clinker, content and composition of mineral components, distribution, crystal size, optical properties, crystallinity, disposition and distribution of crystallites, and void size and distribution) with the specified quality level and the desirable mechanical properties. Additionally, quality

control systems need to be developed in addition to determining the characteristics associated with the desired material.

Unfortunately, Oxygen and Hydrogen are light elements, that are difficult to characterize by X-ray diffraction, SEM/EDX and by TEM/EDX (certainly Hydrogen is impossible to detect by these means). Neutron scattering and diffraction is possible (these methods should allow an investigation into the positions of oxygen and hydrogen atoms in the various phases present in the cement) but the procedure requires a neutron source and thus a reactor.

## G. SCOPE OF THE PRESENT WORK

The purpose of this research is to perform a study of the morphological and crystallographic features of a fully hardened Aalbrog Lion Brand Danish white cement paste with a w/c ratio of 0.25. The reason this particular brand is to be investigated is because it appears to have better toughness properties.

Unfortunately, in the Center for Materials Science and Engineering at NPS, neutron scattering and diffraction facilities are not available and so in this work a study of the phases present and their morphologies was carried out by optical microscopy, x-ray diffraction and scanning and transmission electron microscopy (both with EDX). This work will be done to try and understand why Aalbrog Lion Brand Danish white cement has good mechanical properties.

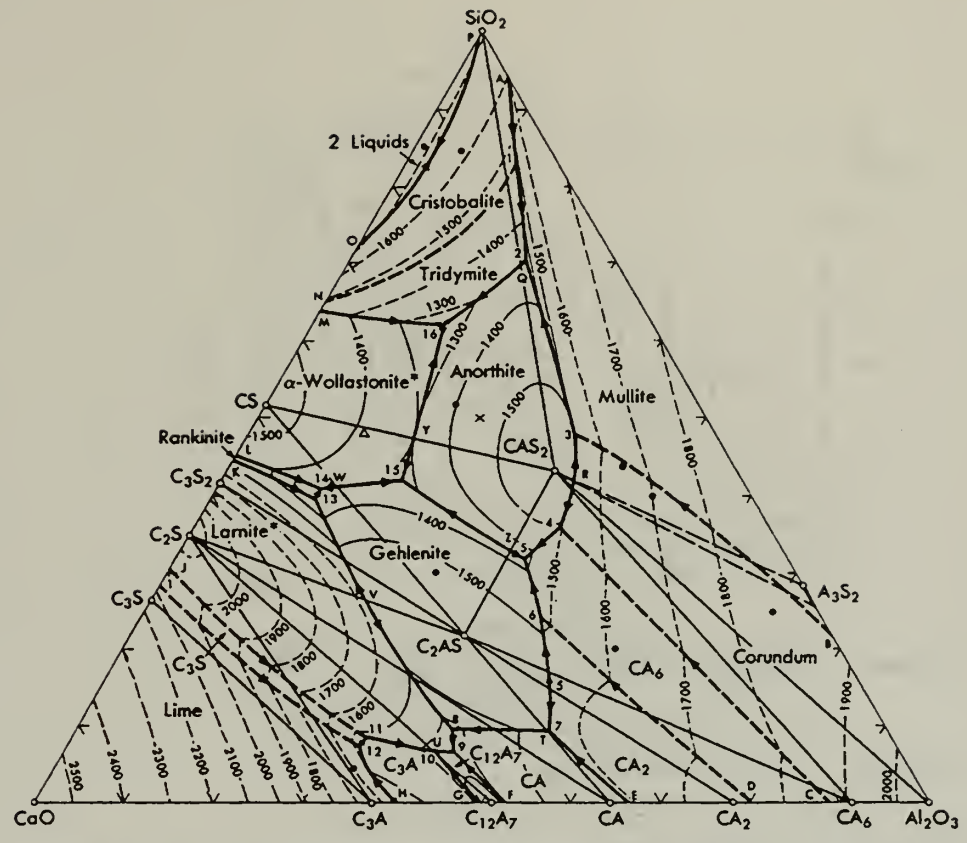


| Compound | Melting temp., °C | Phase name | Composition $Al_2O_3$ | CaO | $SiO_2$ |
|---|---|---|---|---|---|
| A-$Al_2O_3$ | ~2020 | Corundum | 100 | — | — |
| C-CaO | ~2570 | Lime | — | 100 | — |
| S-$SiO_2$ | 1723 | Cristobalite | — | — | 100 |
| S-$SiO_2$ | | Tridymite | — | — | 100 |
| S-$SiO_2$ | | Quartz* | — | — | 100 |
| CS | 1544 | Wollastonite* | — | 48 | 52 |
| $A_3S_2$ | ~1850 | Mullite | 72 | — | 28 |
| $CAS_2$ | 1553 | Anorthite | 37 | 20 | 43 |
| $C_2AS$ | 1593 | Gehlenite | 37 | 41 | 22 |
| $C_3S_2$ | D1 | Rankinite | — | 58 | 42 |
| $C_2S$ | ~2130 | Larnite* | — | 65 | 35 |
| $C_3S$ | D1 | — | — | 74 | 26 |
| $C_3A$ | D1 | — | 38 | 62 | — |
| $C_{12}A_7$ | 1455 | — | 51 | 49 | — |
| CA | ~1605 | — | 64.5 | 35.5 | — |
| $CA_2$ | ~1750 | — | 78.5 | 21.5 | — |
| $CA_6$ | D1 | — | 91.5 | 8.5 | — |

*Name at 25 °C polymorph
D = decomposes

| Invariant Points | Ternary | | | | Binary | | | |
|---|---|---|---|---|---|---|---|---|
| | Temp., °C | $Al_2O_3$ | CaO | $SiO_2$ | | Temp., °C | $Al_2O_3$ | CaO | $SiO_2$ |
| 1 | 1470 | 12 | 5 | 83 | A | ~1590 | 6 | — | 94 |
| 2 | 1345 | 20 | 10 | 70 | B | ~1840 | 78 | — | 22 |
| 3 | 1512 | 37 | 15 | 48 | C | ~1850 | 89 | 11 | — |
| 4 | 1495 | 41 | 23 | 36 | D | ~1730 | 80 | 20 | — |
| 5 | 1380 | 39 | 29 | 32 | E | ~1595 | 66.5 | 33.5 | — |
| 6 | 1475 | 45 | 31 | 24 | F | 1400 | 53 | 47 | — |
| 7 | 1500 | 53 | 37.5 | 9.5 | G | 1395 | 50 | 50 | — |
| 8 | 1380 | 42 | 48.5 | 9.5 | H | 1535 | 41 | 59 | — |
| 9 | 1335 | 43.5 | 49.5 | 7 | I | ~2070 | — | 72 | 28 |
| 10 | 1335 | 41.5 | 52 | 6.5 | J | ~2050 | — | 70 | 30 |
| 11 | 1455 | 33 | 58.5 | 8.5 | K | 1464 | — | 55.5 | 44.5 |
| 12 | 1470 | 33 | 59.5 | 7.5 | L | 1460 | — | 55 | 45 |
| 13 | ~1315 | 12 | 49 | 39 | M | 1436 | — | 36 | 64 |
| 14 | ~1310 | 12 | 47 | 41 | N | 1470 | — | 35 | 65 |
| 15 | 1266 | 20 | 38 | 42 | O | 1707 | — | 27 | 73 |
| 16 | 1170 | 15 | 23 | 62 | P | 1707 | — | 1 | 99 |
| | | | | | Q | 1368 | 19.5 | 11.5 | 70 |
| | | | | | R | 1547 | 39.5 | 18.5 | 42 |
| | | | | | S | 1552 | 50 | 35 | 15 |
| | | | | | T | 1512 | 52.5 | 38 | 9.5 |
| | | | | | U | 1335 | 41 | 52.5 | 6.5 |
| | | | | | V | 1545 | 24 | 50 | 26 |
| | | | | | W | 1318 | 13 | 46 | 41 |
| | | | | | Y | 1307 | 37 | 30 | 33 |
| | | | | | Z | 1385 | 19 | 34 | 47 |

Figure 2.1 The $CaO$-$Al_2O_3$-$SiO_2$ system (from Ref. 6).

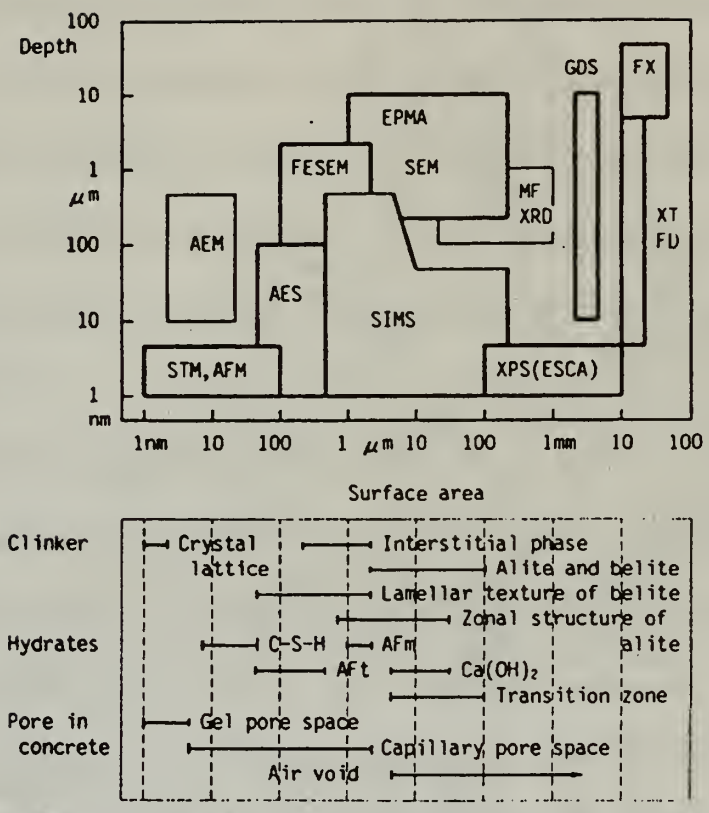


AEM: Analytical Transmission Electron Microscope, STM: Scanning Tunnel Microscope, AFM: Atomic Force Microscope, AES: Auger Electron Spectroscope, FESEM: Field Emission Scanning Electron Microscope, EPMA: Electron Probe Micro Analyzer, SIMS: Secondary Ion Mass Spectroscope, XPS(ESCA): X-ray Photoelectron Spectroscope, MFXRD: Micro Focus X-ray Diffractometer, GDS: Grow Discharge Spectrometer, XTFD: X-ray Thin Film Diffractometer, FX: Fluorescent X-ray Spectrometer

Figure 2.2 Measuring range of each surface and local characterization instruments (from Ref. 14).

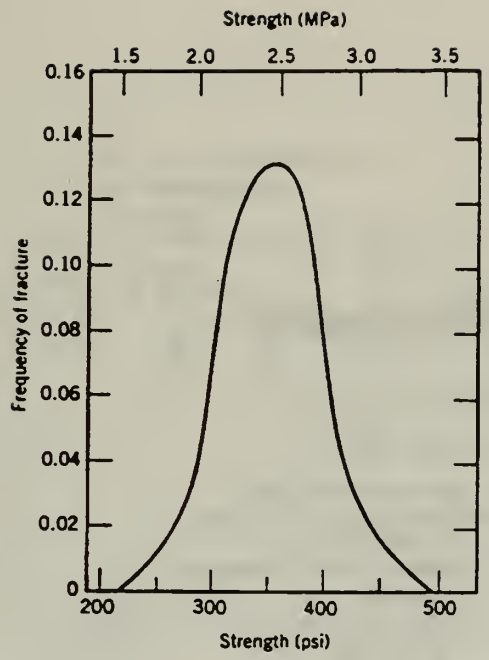


Figure 2.3 The frequency distribution of observed fracture strengths for a typical portland cement (from Ref. 5).

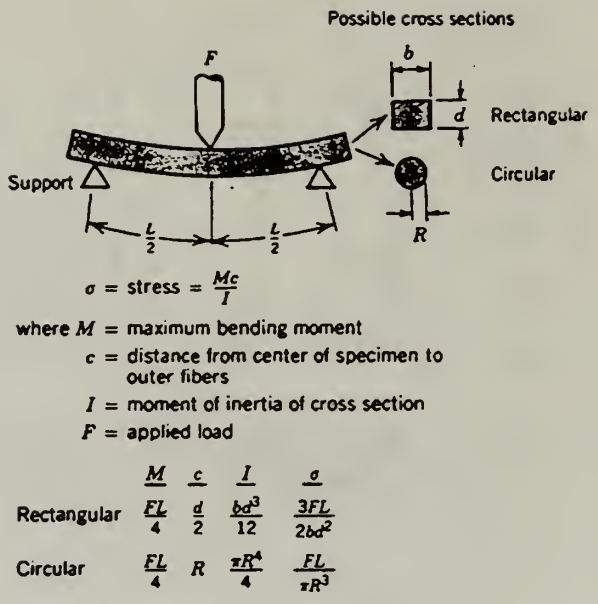


Figure 2.4 A three-point loading scheme to measure the stress-strain behavior and modulus of rupture of ceramics (from Ref. 5).

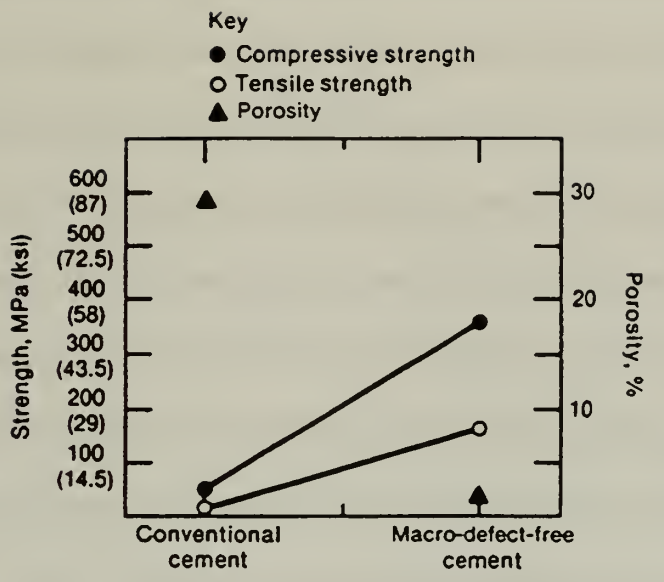


Figure 2.5 Increases in strength and decreases in porosity achieved with advanced macro-defect-free (MDF) cements (from Ref. 13).

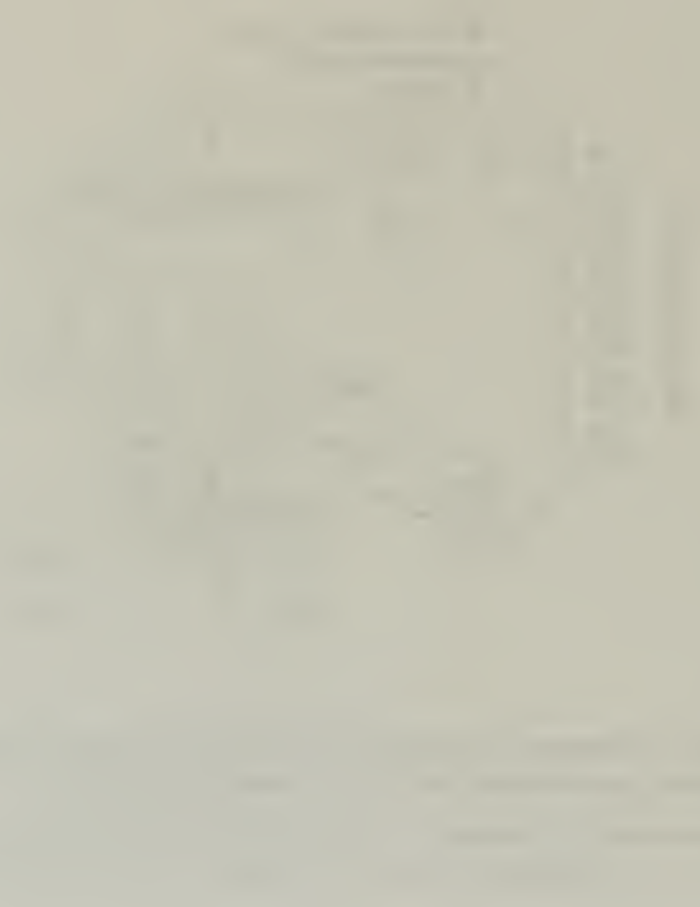

# III. EXPERIMENTAL PROCEDURE

## A. SAMPLE DESCRIPTION

One specimen (D230) was forwarded from the Nuclear Science and Technology Organization (ANSTO), Australia for analysis. The sample was fabricated from Aalbrog Lion Brand Danish white cement mixed with deuterated water at room temperature on a shaker to prepare cement pastes at nominal water: cement (w/c) ratios of 0.25. After mixing the specimens were demolded and cured for a period of one year. Deuterated water was used so that neutron scattering and diffraction studies could be performed elsewhere. Table 3-1 contains the chemical analysis of the sample as weight-percent oxide and its mineralogical compositions calculated from the chemical composition by Bogue calculations. Table 3.2 contains a quantitative x-ray analysis of the cement before hydration.

## B. SAMPLE PREPARATION

Sectioned samples were grit sanded using a Struers Knuth-Rotor-3 and various grits of waterproof silicon carbide paper. The SEM samples were polished with great care, using one micron water based diamond compound on selvyt polishing Microcloth, while all other samples remained in the as sectioned condition for additional work. Care was taken to avoid overpolishing the sample at each stage, so the details of the delicate structure were to be properly revealed. The SEM samples were then transferred to an Ernest Fullam EFFA MKII carbon coater where two carbon strands at a distance of

approximately 30 millimeters from the sample surface were used to impart a uniform 15-20 nm coating of the specimen surface so that it was conducting for SEM studies.

The X-ray diffraction (XRD) samples were taken from the sectioned samples described above. The samples were hand ground in an agate mortar and sieved through a 400 mesh (38 μm) sieve. The resulting fine powder was then used for the x-ray diffraction experiments.

An additional sample was ground in the agate mortar and sieved for electron microscopy (TEM). The resulting powder was placed into a bath of ethanol and stirred. Next, a carbon-coated 400 mesh copper grid was used to scoop the powder particles so that they were suspended on the grid. The sample was then carefully lifted from the solvent and air dried.

Additionally, specimens for transmission electron microscopy (TEM) were made by mounting small slices on a glass slide and polishing these down to approximately 20 μm thickness. The polished samples were then cored to form 3mm diameter discs using a precision coring tool with a diamond core drill. The 3 mm diameter disk samples generated in this way were then mounted on 1.5 mm aperture Copper grids. These were then argon ion-beam milled until the center of the samples had thinned to a hole. Most of the regions around the holes in the ion milled samples were electron transparent. Thinning was at rates of $< 2.5$ μm $h^{-1}$ and included the use of a liquid nitrogen-cooled cold stage to help minimize thermal damage (as suggested by Richardson and Groves [10]).

## C. LOSS ON IGNITION

The non-evaporable water contents of the furnace fired samples were determined by measuring the loss on ignition at 1050° C. The average results of two runs were obtained, based on the fired weight. The experimental procedure was as follow:

(1) The weighed samples were fired at 1050° C for approximately 19 hours.

(2) Samples were then weighed immediately after removal from the furnace and loss on ignition calculated. The dehydrated samples were then immediately studied by x-ray diffraction.

(3) The water content was determined to be approximately 24 weight percent, which suggests that the hydrated cement is an equimolar mixture of approximately $Ca_{1.75}.SiO_2.3H_2O$ and $Ca(OH)_2$.

## D. SCANNING ELECTRON MICROSCOPY

The polished and coated samples were placed for analysis in the TOPCON SM-510 scanning electron microscope (SEM) with a tungsten filament energized to 20,000 volts. Polished surfaces were used for the determination of the phase distribution by backscattered electron imaging and chemical composition. X-ray microanalysis (EDS) was used to provide quantitative spot chemical analysis as well as maps of the distribution of the elements present. Analysis was conducted at 1000 times magnification with a working distance of 28.5 mm.

## E. TRANSMISSION ELECTRON MICROSCOPY

A TOPCON EM-002B transmission electron microscope (TEM) with $LaB_6$ source energized to 200 kV was used for the microstructural and chemical characterization of several samples of the hydrated cement. As described above, the samples were placed on a 400 mesh copper TEM grid and conventional TEM micrographs and selected area diffraction patterns were taken from many sample regions. The samples were tilted 10 degrees toward the EDX detector so that x-ray counts approaching 1000 c.p.s. could be obtained with a small (~ 16 nm) probe size. The EDAX system has a super ultra thin window so that light elements down to boron can be detected. The EDX data was analyzed using EDAX/EDX software. Quantitative analysis of these thin specimens was performed without the need for absorption and fluorescence corrections. The specimens were sufficiently thin and so these could be ignored.

## F. OPTICAL MICROSCOPY

A Zeiss Jenaphot 2000 optical microscope was used to obtain micrographs of the polished sample surfaces. This was used for qualitative comparison of the specimen macrostructure. In particular, equiaxed white and grey particles were observed by optical microscopy and these proved to be very important when the material was studied in the SEM. Observation were conducted at 125 times magnification.

## G. X-RAY DIFFRACTOMETRY

All samples were analyzed utilizing a Phillips XRG 3100 X-Ray Generator and a PW-3020 Diffractometer Controller. The data processing was performed using a DEC 3100

Vax Workstation. X-ray diffraction patterns were collected using an x-ray generator with a copper target ($K\alpha_1$ and $K\alpha_2$ wavelengths 1.54060 and 1.54439 A°) and a bent graphite crystal monochromator. The operating parameters were as follows: 30 Kv, 35 mA, angle range 5 - 140° and scan rate of 5 seconds per every 0.02 degree increment.

The acquired data was processed by the Phillips APD 1700 software on the Vax workstation 3100. Spectral plots of intensity versus $2\theta$ position were plotted for all samples. The Phillips PW 1891 Total Access Diffraction Database (TADD) compared sample plots with library diffraction patterns at an extremely rapid rate. Several crystalline phases were detected and library intensity histogram diffraction patterns were plotted for comparison with spectral plots. The crystalline phases were determined using the TADD in conjunction with the Joint Committee on Power Diffraction Standards (JCPDS) x-ray diffraction data cards.

(a)

| Chemical composition | Oxide content: wt.% |
|---|---|
| $SiO_2$ | 24 |
| $Al_2O_3$ | 1.9 |
| $Fe_2O_3$ | 0.3 |
| CaO | 70 |
| MgO | 0.6 |
| $SO_3$ | 1.9 |

(b)

| Calculated compounds | Bogue content: wt% |
|---|---|
| $C_3S$ | 82 |
| $C_2S$ | 8 |
| $C_3A$ | 4 |
| $C_4AF$ | 1 |

Table 3-1. (a) Chemical composition; and (b) Bogue calculations for sample D230. (Provided by ANSTO)

| Calculated composition | Quantitative x-ray content wt.% |
|---|---|
| $C_3S$ | 80 |
| $C_2S$ | 15 |
| $C_3A$(cubic) | 3 |
| $C_3A$(monoclinic) | 1 |
| $C_4AF$ | 1 |

Table 3.2 Quantitative x-ray analysis for sample D230 (anhydrous). (Provided by ANSTO)

# IV. RESULTS AND DISCUSSION

## A. LOSS ON IGNITION

In order to obtain the formula for the amorphous phase (C-S-H gel) from the loss on ignition results, an average $CaO/SiO_2$ ratio of 1.75 was assumed for the resulting C-S-H. In addition, the $Al_2O_3$ content of the cement was ignored because very little is present; it was also assumed that the reaction has proceeded to completion with anhydrous components absent after reaction. The expected formula in the reaction was calculated by converting the weight percentage of mixed constituents to molecular percent. This calculation indicated that the hydrated material is comprised of equimolar amounts of $1.75CaO.SiO_2.3H_2O$ and $Ca(OH)_2$.

The difference between the two loss on ignition runs were not significant. They indicate that more likely both samples have been equally hydrated, with no difference in the extent of the chemical reactions between the cement and the water.

## B. X-RAY DIFFRACTION

The powdered hydrated cement and oven fired cement samples were analyzed using X-ray diffraction in order to determine the phases present and any changes resulting from the heat treatment and exposure to the environment. Figure 4.1 illustrates the x-ray diffraction patterns of the crystalline and noncrystalline phases in the as received and hydrated powder sample. All the distinguishable intensity peaks were identified by using the Phillips APD 1700 software package in conjunction with the Hanawalt JCPD diffraction patterns data cards. The Miller indices were obtained from X-ray Diffraction

Data Cards published by the Joint Committee on Chemical Analysis by X-ray Diffraction Methods (October 1955).

Amorphous C-S-H (close-to amorphous) was found to be the main phase present. This is indicated by the almost amorphous shape (background hump) from 2θ equal to 25° to 2θ equal to 60°. Peaks or bands from C-S-H gel occur at *d*-spacings of 3.2 - 2.6, 0.182 and 0.156 nm, with low angle scattering but no other definite peaks between 2θ equal to 15° and *d*-spacing of 0.13. No other crystalline phases present in this particular cement will have peaks or an amorphous shape at those 2θ values. However, the C-S-H apparently has several other crystalline phases within the amorphous matrix, which are illustrated in Figure 4.2. The figure also shows a copy of the JCPDS card for a paste of β-$C_2S$ that was published by Mohan and Taylor. The card shows a diffuse peak between *d*-spacings of 0.279 and 0.310 nm and a well defined peak at 0.182 nm. The broad peaks are indicative of wide distributions of *d*-spacing, indicating the lack of a unique structural order and the possibility of a structure that could be highly variable at the submicron level, as we will see later in the TEM analysis. The sharper peaks near 2θ equal to 28°, 29°, 33°, 35°, 42°, 47°, and 52°, are characteristic of most materials containing silicate or traces of CaO (Viehland and Li (1996)), further confirming the presence of the crystalline phases ($Ca(OH)_2$ and $C_3S$ or β-$C_2S$) within the amorphous matrix.

The powder samples analyzed indicated other phases present, for which the expected peak intensity and line positions accurately reflected the Hanawalt JCPDS diffraction patterns, verifying the phases present. Figures 4.3 and 4.4 show the x-ray diffraction

pattern for the as-received and hydrated sample compared with the JCPDS diffraction patterns of the major components expected in the sample. Each components maximum intensity line is properly identified. Portlandite ($Ca(OH)_2$) has a peak intensity at the (001) reflecting plane, $Ca_3SiO_5$ peak intensity at (111) and (201), Larnite ($Ca_2SiO_4$) at ($\bar{1}01$), CaO at (111) and Ettringite $Ca_6Al_2(SO_4SiO_4CO_3)_3(OH)_{12}.26H_2O$ at (002). The amount of Larnite is very small as expected.

The XRD pattern for the fired (used for the loss on ignition test) sample is shown in Figure 4.5. The figure shows a comparison with the JCPDS diffraction patterns on the major components identified in the fired sample. The sharper peaks are identified as $C_3S$ at $2\theta$ equal to 29° and 32°, $\beta$-$C_2S$ at 32.5°, 34° and 42°, and CaO at 37° and 53.5°. The presence of $C_3S$ and $\beta$-$C_2S$ is caused by the dehydration of C-S-H, whereas the presence of CaO is due to the dissociation of $Ca(OH)_2$, which is in perfect agreement with the loss on ignition experiment.

This crystallographic data is in excellent agreement with the SEM/EDX data (described below) and it is in excellent agreement with previous x-ray work on this topic [17, 18, 19, 20] although it still does not allow for the resolution of micro and nanocrystalline phases that could be within the C-S-H matrix. For this, SEM and TEM experiments are necessary.

## C. OPTICAL AND SCANNING ELECTRON MICROSCOPY (SEM)

A low magnification optical micrograph from a polished cross section of the specimen (sample D230), showing the sample morphology is presented in Figure 4.6. The

micrograph shows 'white' equiaxed particles with sizes varying from a few microns to many tens of microns in a light grey matrix. The morphological characteristics illustrated in the micrograph, are typical for most hydrated cements, of any age or w/c ratio.

A higher magnification backscattered scanning electron micrograph shown in Figure 4.7, reveals a surface morphology having what appears to be the same 'white' particles observed in the optical microscope and these often have 'light grey' surroundings. These particles are embedded throughout a darker and finer 'grey' matrix. Since the backscattered detector detects difference in atomic number, a quantitative phase analysis of each region could be attempted. The 'white' particles have the highest average atomic number and the 'dark grey' matrix the lowest with the 'light grey' in between. A microchemical analyses of the individual regions by energy-dispersive x-ray analysis (EDXA), provided a better appreciation of the differences in the composition of each region. The analyses (in atomic %) are presented in Table 4.1. The equiaxed, 'white' phase is very bright and this suggests that it does not contain much water (if any) and the EDXA analysis indicates that the 'white' regions have a formula of $3CaO.SiO_2$. This analysis suggests these regions are anhydrous $C_3S$, which is in complete agreement with the previous findings of Diamond [12] and Meredith [11] and also with the XRD results presented in Figure 4.3 and 4.5. The $C_3S$ phase appears much brighter than the surrounding 'light grey' and matrix phases because it has a higher average molecular weight and does not contain water. The chemical analysis shown in Table 4.1 clearly demonstrates the fact that the 'white' phase is richer in calcium when compared to the

surrounding 'light grey' phase. This is expected since there is a 3:1 calcium to silicon atomic ratio in the $Ca_3SiO_5$ ($C_3S$) phase and an average 2:1 ratio in the 'light grey' region (this region would appear to be comprised of a mixture of C-S-H and CH). The chemical analyses of the darker phase suggests that the 'dark grey' phase has a higher average atomic number than the 'light grey' phase, which is opposite to that indicated by the backscattered imaging. The reason for this is that the 'dark grey' phase (the somewhat cellular matrix) is more hydrated (the effective backscatter coefficient of the phase is reduced by the nonevaporable water in its structure) than the 'light grey' phase and the EDXA does not detect hydrogen. In addition to C-S-H and calcium hydroxide (CH), the 'dark grey' matrix would also seen to contain small amounts of ettringite, Larnite, and some impurities, as well as a great deal of porosity. This is in excellent agreement with the XRD data shown in Figures 4.1 and 4.2, and also with previous findings of Diamond [12].

**D. TRANSMISSION ELECTRON MICROSCOPY**

Examination of the as-received hydrated cement thin foil in the TEM revealed, as expected, a matrix which was a mixture of several phases and crystalline regions. Figure 4.8 shows a bright-field image taken of the C-S-H gel phase of the hydrated cement. Following the results obtained above and the designation of previous studies, [9] regions of inner product (light grey in the SEM micrographs) and outer product (dark grey in the SEM micrographs) were identified. This micrograph was taken from an outer product area and had a morphology similar to the type described by Viehland [9], for an outer

product region. The morphological characteristics of this outer product region are "honeycomb-like", which is indicative of C-S-H phases formed under constrained conditions [9, 10]. EDXA (Figure 4.9) analysis revealed an average Ca:Si ratio of 1.76 in addition to traces of aluminum and sulfur, no magnesium was detected by TEM, which is in agreement with the results obtained by Richardson [10], for an outer C-S-H region. The SAED pattern for this region is shown in Figure 4.10. The pattern contains diffuse rings which clearly demonstrate the presence of nanocrystalline regions coexisting with the amorphous C-S-H phase; such regions have been detected by other workers [9]. Figure 4.11 is also a bright-field image taken from an inner product area, showing a somewhat compact and homogeneous fine scale ("featureless") morphology. These results are consistent with previous investigations, [9, 10, 12] indicating, that at the nanometer scale, this brand of Danish white cement is somewhat similar to specimens used by other investigators.

In general, cements have been classified by the period of hydration during which they form. The morphology of the outer C-S-H regions (formed within the first 24 hours of hydration) is fiber (needle) -like if sufficient space is available for growth [10]. However, if the space available is constrained (as would seen to be the case for the present case), an equiaxed ("honeycomb-like") microstructure can develop. The morphology of the inner C-S-H regions (formed after 24 hours hydration) appears to be featureless on the micrometer scale. The principal condition of formation responsible for the observed

morphological differences threfore appears to be the internal stress state in which this cement paste was formed.

Figures 4.12 and 4.13 show an inner/outer product interface region for the C-S-H gel. The interface bonding is generally very strong, with a poorly defined morphology. The interface in the top right-hand quarter of Figure 4.12, appears at first glance to be somewhat well defined, but on examination at higher magnification (Figure 4.13), the inner C-S-H seems to extend pasts its boundary. The interfaces in the other regions of the micrographs overlap even more, rendering them morphologically indistinguishable.

The presence of unhydrated $C_2S$ is demonstrated in Figure 4.14. $C_2S$ is the large striated region at the top of the micrograph, which appears to be partly hydrated (EDXA for this region is shown in Figure 4.15(a)). Twins are clearly visible in this micrograph and probably preexisted in the original $\beta$-$C_2S$, which is in perfect agreement with the results previously obtained at the micrometer scale by Diamond [12]. The micrograph also shows a region of inner C-S-H, for which the EDXA is shown in Figure 4.15(b).

EDXA was also used to determine the local composition of various regions throughout the C-S-H gel. The quantitative analysis indicated that the Ca:Si ratio fluctuated between 0.35 and 5.74. The degree of fluctuation in the Ca:Si ratio observed is similar to that previously reported by Viehland and Li [9]. The Ca:Si ratio normally fluctuates between 0.6 and 2.0 when the C-S-H is studied with a large probe size [10]. Viehland and Li attribute the wider fluctuations observed to the small beam size used (their spot size was 1nm). In this study a 16 nm spread probe, was generally used, to

prevent beam damage. However, a 6nm probe was used to study local variation in the composition. Consequently, the magnitude of the Ca:Si fluctuation in this case, may be attributed to the growth of C-S-H and CH on the nanometer scale. In general, the magnitude of the fluctuations was much larger than the results obtained for the probed regions on the micrometer scale, which is in agreement with previous investigations. The EDX analysis showed that the aluminum and sulfur levels were low for all the regions of the C-S-H gel investigated. Of these, aluminum is generally considered the most significant of the minor elements present. Unfortunately, EDXA has problems in establishing the true levels of aluminum in the C-S-H gel, due to the C-S-H gel beam-sensitivity.

The stability of the hydrated specimen to irradiation damage was checked during observations in the TEM. Standardized conditions for sample preparation and observation (large beam defocus) were used, as previously suggested by Richardson and Groves [10]. However, when the beam was focused on a single crystalline region, damage was observed. In addition, there were problems with selective evaporation during the observation because the EDAX count rate was varying with time. In general, it was observed that the stability increased in regions with lower Ca:Si ratios, as previously reported by Richardson [10].

Figures 4.16 and 4.17 shows several SAD patterns obtained from various randomly selected regions within the gel. Diffuse rings, similar to the rings observed by Viehland, were discovered in all three patterns. The presence of these rings suggest that the local

structure is not completely disordered, and that short-range ordering exists, as suggested by our XRD results. The broad diffuse rings were measured after the TEM camera length was calibrated. In Figure 4.16(a) the inner diffuse ring was measured, and the inner edge of the ring was found to have a *d*-spacing of 0.34 nm and the outer edge of the ring a *d*-spacing of approximately 0.28 nm, which are very similar to the results obtained by Viehland [9], during his analysis of a Portland cement with a w/c ratio of 0.4. The broad diffuse rings are indicative of the structural variations within short-range ordered regions, which are consistent with the XRD results. As mentioned before, the XRD data did suggest the presence of broad diffuse peaks or bands in the range of approximately 0.32 - 0.26 nm. Examination of Figures 4.16 and 4.17 shows that the periodicity of the diffuse rings varies from one region to the other. The range for the first ring in Figure 4.16(b), is 0.31 nm for the inner edge and 0.262 nm for the outer edge, whereas for Figure 4.17 the range is 0.243 - 0.213 nm. Inspection of Figure 4.16(b) shows that the second diffuse ring has a periodicity of 0.243 nm. A third ring follows after a gap, for which the periodicity is ~ 0.179 nm, which is similar to the expected repeat distance for $Ca(OH)_2$. The ordering described, confirms the presence of the hexagonal lattice of C-H within the regions from which the patterns were taken (C-S-H gel). In addition, an inspection of the EDX data corresponding to the regions from which the diffraction patterns were taken, resulted in Ca:Si fluctuations that could be related to the degree of short-range ordering, as suggested by previous investigators.

The presence of CH within the C-S-H gel, was also detected using SAD with EDX analyses, as illustrated in Figures 4.18 - 4.20. Figure 4.18 shows a bright-field image (taken from the powder particles suspended on a copper grid) in which regions of C-S-H and CH are identified. Figure 4.19(a) shows an EDX analysis of the C-S-H region, whereas Figure 4.19(b) shows the EDX analysis of the CH region. Because hydrogen is not detected by EDX, the analysis confirmed that only calcium and oxygen were present in the CH region, as shown in Figure 4.19(a). The EDX analysis of the C-S-H region, showed the presence of calcium and silicon at an average Ca:Si ratio of 2.12, as shown in Figure 4.19(b). The SAED for the CH region is shown in Figure 4.20 (the electron beam direction is [110]). The *d*-spacings observed in this pattern are 0.28, 0.24, 0.17, 0.14, and 0.11 nm, which correspond to the [111], [200], [220], [311], and [331] reflections, respectively. These results correspond to what is expected for the CaO repeat distance, as stated in the JCPDS card. However, this type of pattern could be attributed to a pseudohexagonal lattice, which could be approximated to hexagonal CH, as suggested by previous investigators [9]. These results confirm the presence of CH within the C-S-H gel (intermixed with C-S-H), which can cause the Ca:Si ratio in the C-S-H gel to be higher in the regions where the CH is more concentrated. This is consistent with the observations made concerning the Ca:Si ratio fluctuation.

| | O | Al | Si | S | Ca |
|---|---|---|---|---|---|
| White | 53.68 | 0.51 | 11.31 | - | 34.78 |
| Light Grey | 66.86 | 0.32 | 9.16 | 0.95 | 22.72 |
| Dark Grey | 64.39 | 1.18 | 8.64 | 0.68 | 25.11 |

Table 4.1 EDX results for the three regions (in atomic %) White, Light Grey and Dark Grey. Notice that no hydrogen can be detected by EDX.

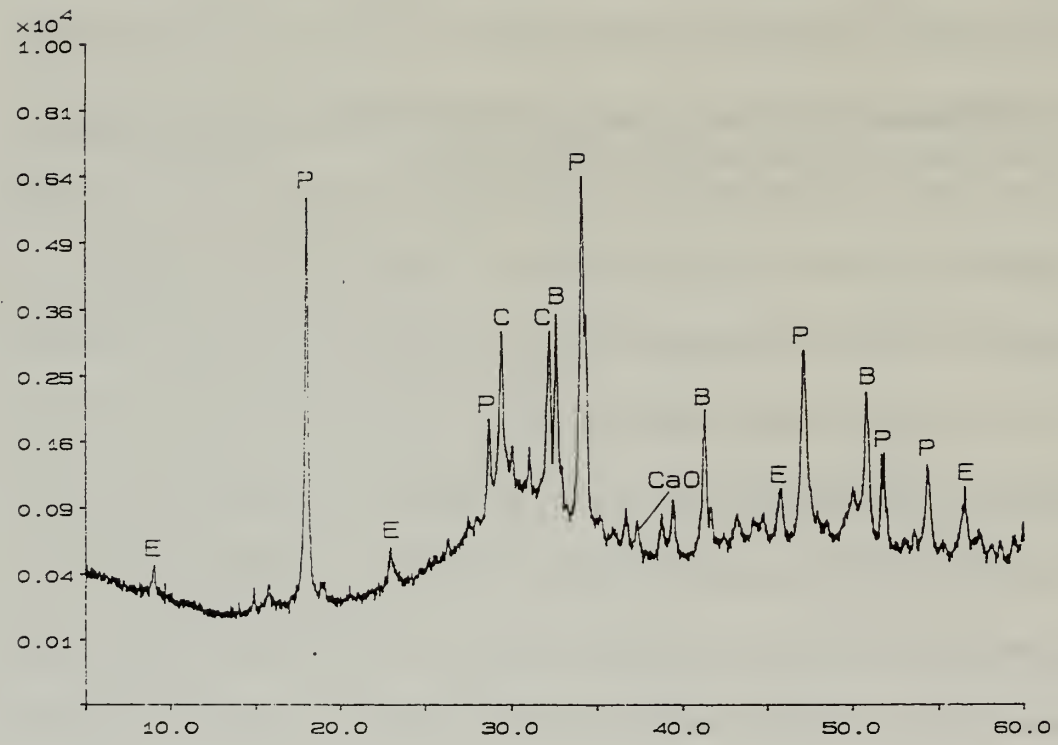


Figure 4.1 XRD Pattern of the as-received and hydrated powder sample showing crystalline phases E=Ettringite, P=Portlandite, C=$C_3S$, B=$\beta$-$C_2S$, and CaO.

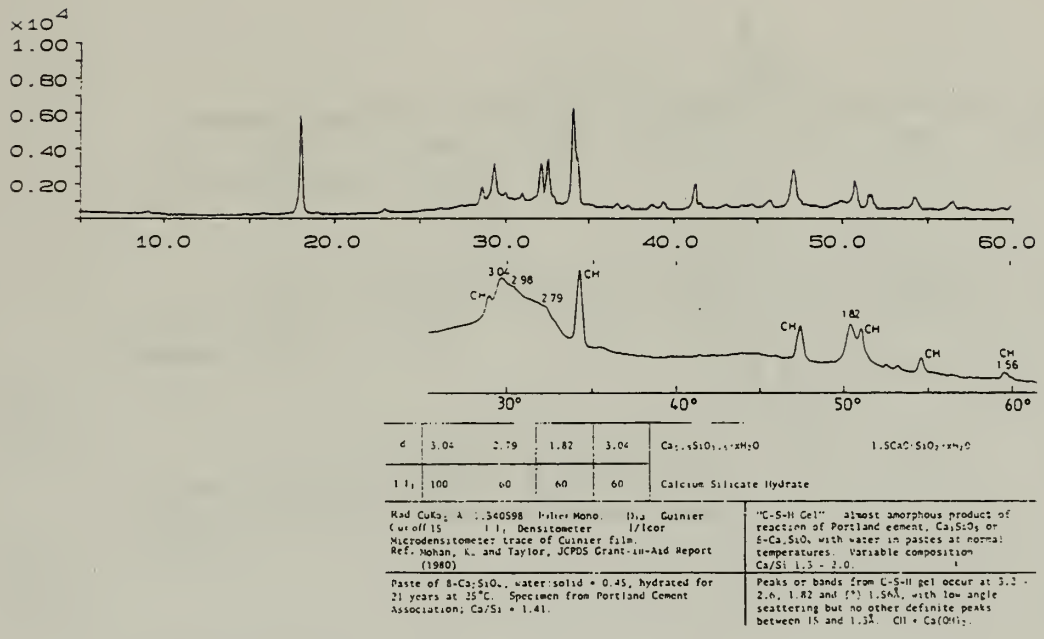
×10^4
1.00
0.80
0.60
0.40
0.20
10.0
20.0
30.0
40.0
50.0
60.0
CH
3.04
2.98
2.79
CH
CH
1.82
CH
CH
CH
1.56
30°
40°
50°
60°
d 3.04 2.79 1.82 3.04 Ca1.xSiO3.1-xH2O 1.5CaO·SiO2·xH2O
I/I1 100 60 60 60 Calcium Silicate Hydrate
Rad CuKα1 λ 1.540598 Filter Mono. Dia Guinier
Cut off 15 I/I1 Densitometer I/Icor
Microdensitometer trace of Guinier film.
Ref. Mohan, K. and Taylor, JCPDS Grant-in-Aid Report (1980)
"C-S-H Gel" almost amorphous product of reaction of Portland cement, Ca3SiO5 or β-Ca2SiO4 with water in pastes at normal temperatures. Variable composition Ca/Si 1.5 - 2.0.
Paste of β-Ca2SiO4, water:solid = 0.45, hydrated for 21 years at 25°C. Specimen from Portland Cement Association; Ca/Si = 1.41.
Peaks or bands from C-S-H gel occur at 3.2 - 2.6, 1.82 and [?] 1.5Å, with low angle scattering but no other definite peaks between 15 and 1.3Å. CH = Ca(OH)2.

Figure 4.2 XRD Pattern of the as-received and hydrated powder sample showing the amorphous C-S-H phase from 2θ=25° to 2θ=60°. A copy of the JCPDS card is also illustrated.

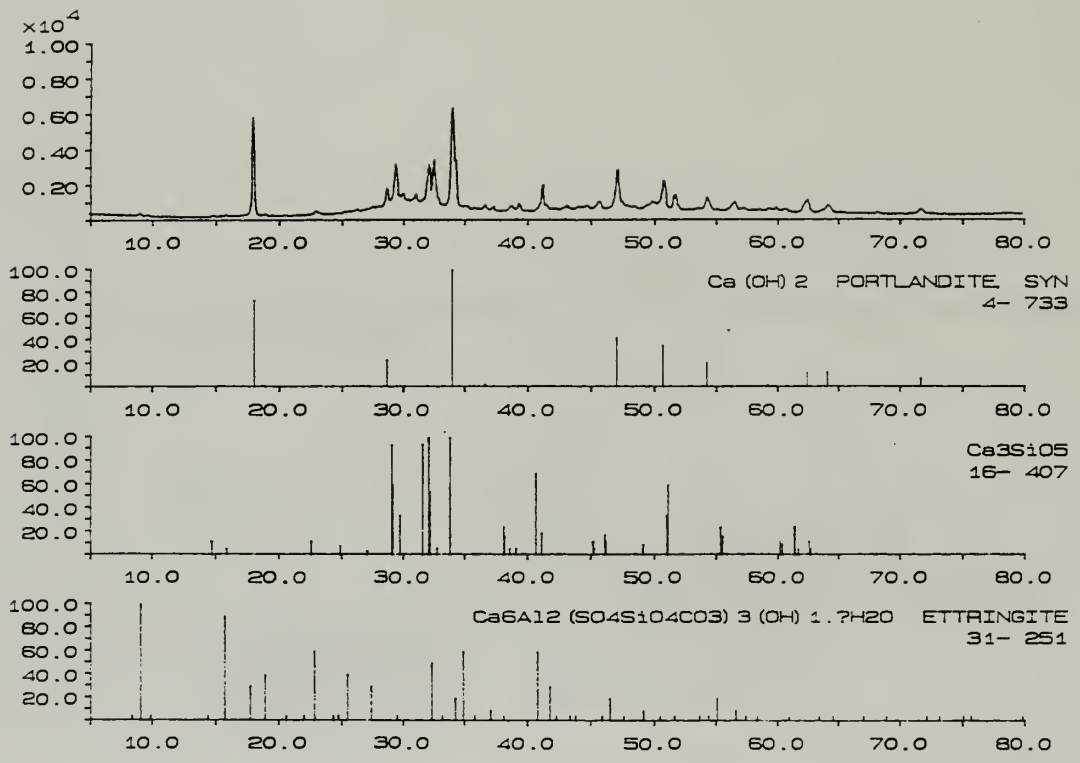


Figure 4.3 XRD line patterns of phases present in the as-received and hydrated powder sample.

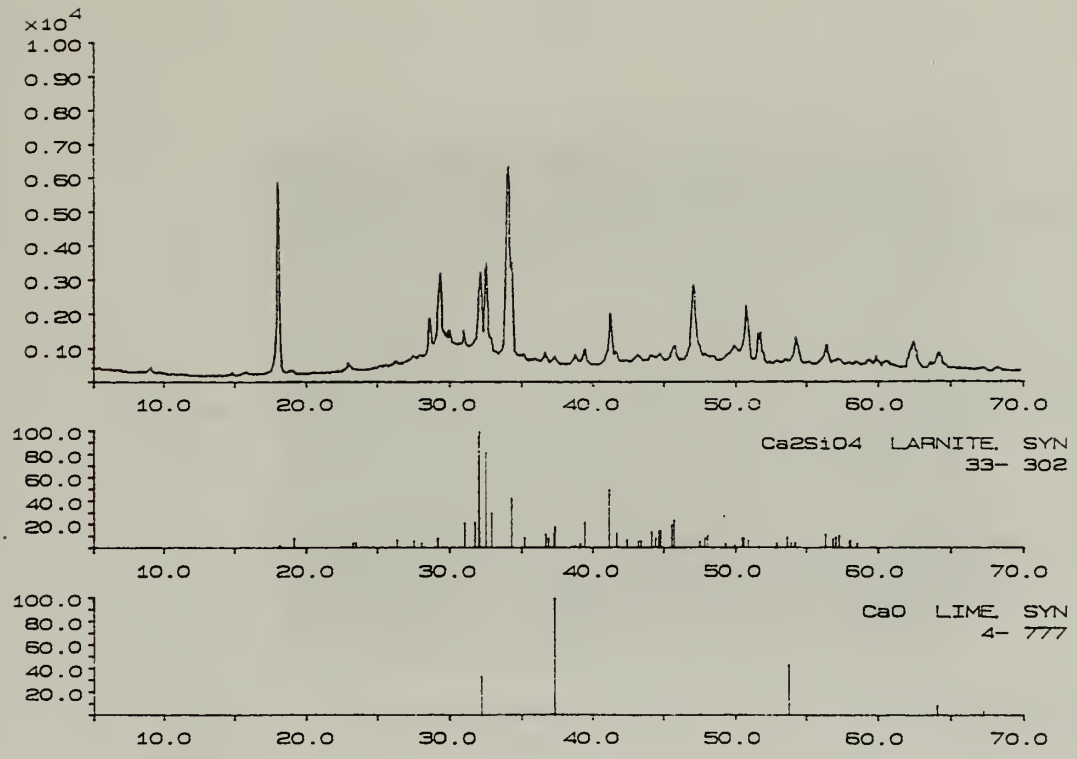


Figure 4.4 XRD line patterns of phases present in the as-received and hydrated powder sample.

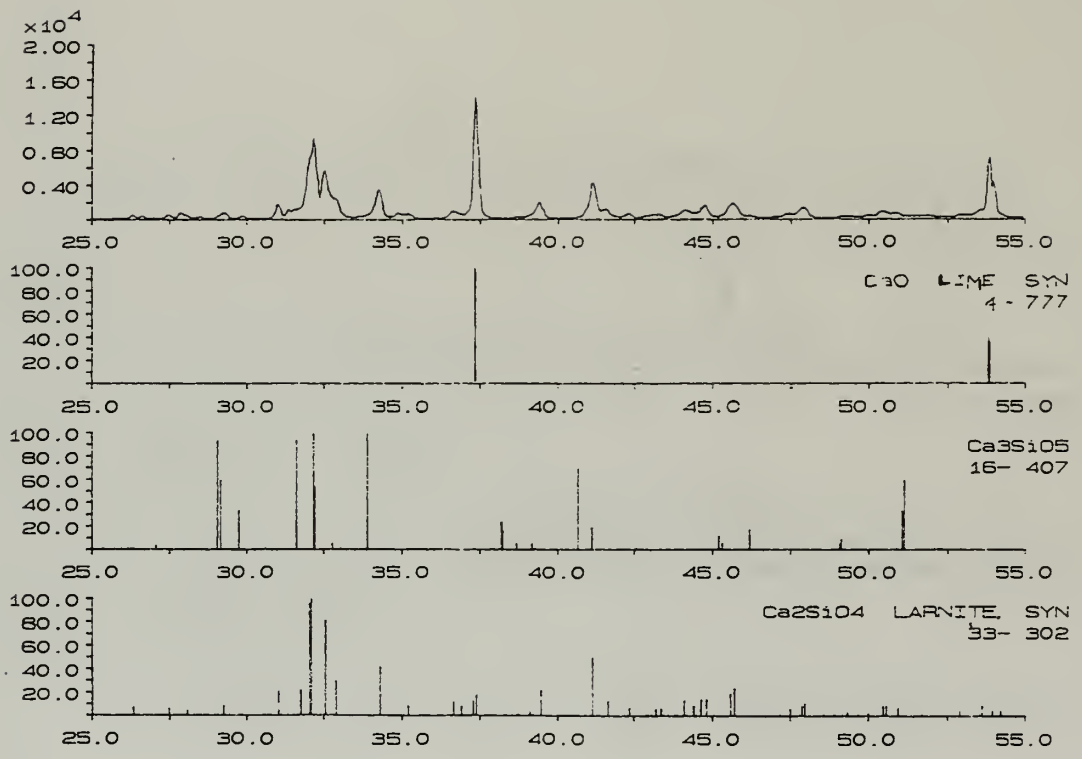


Figure 4.5 XRD line patterns of phases present in a fired sample used for the loss on ignition test.

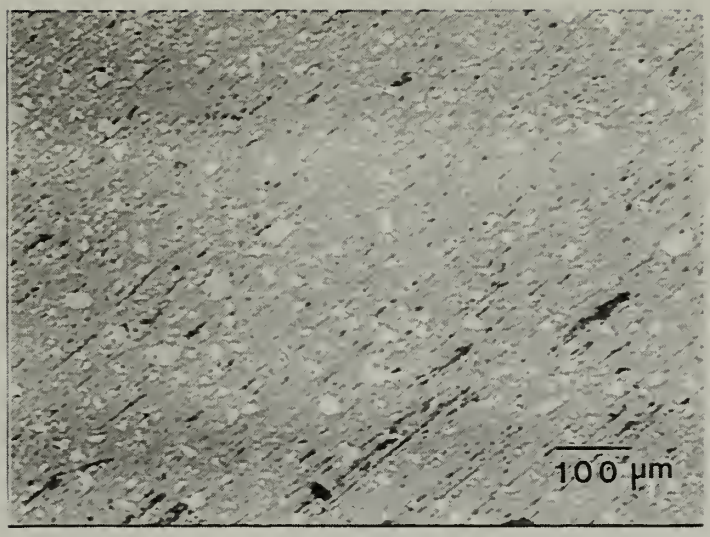


Figure 4.6 Optical Micrograph of the as-received and hydrated powder sample.

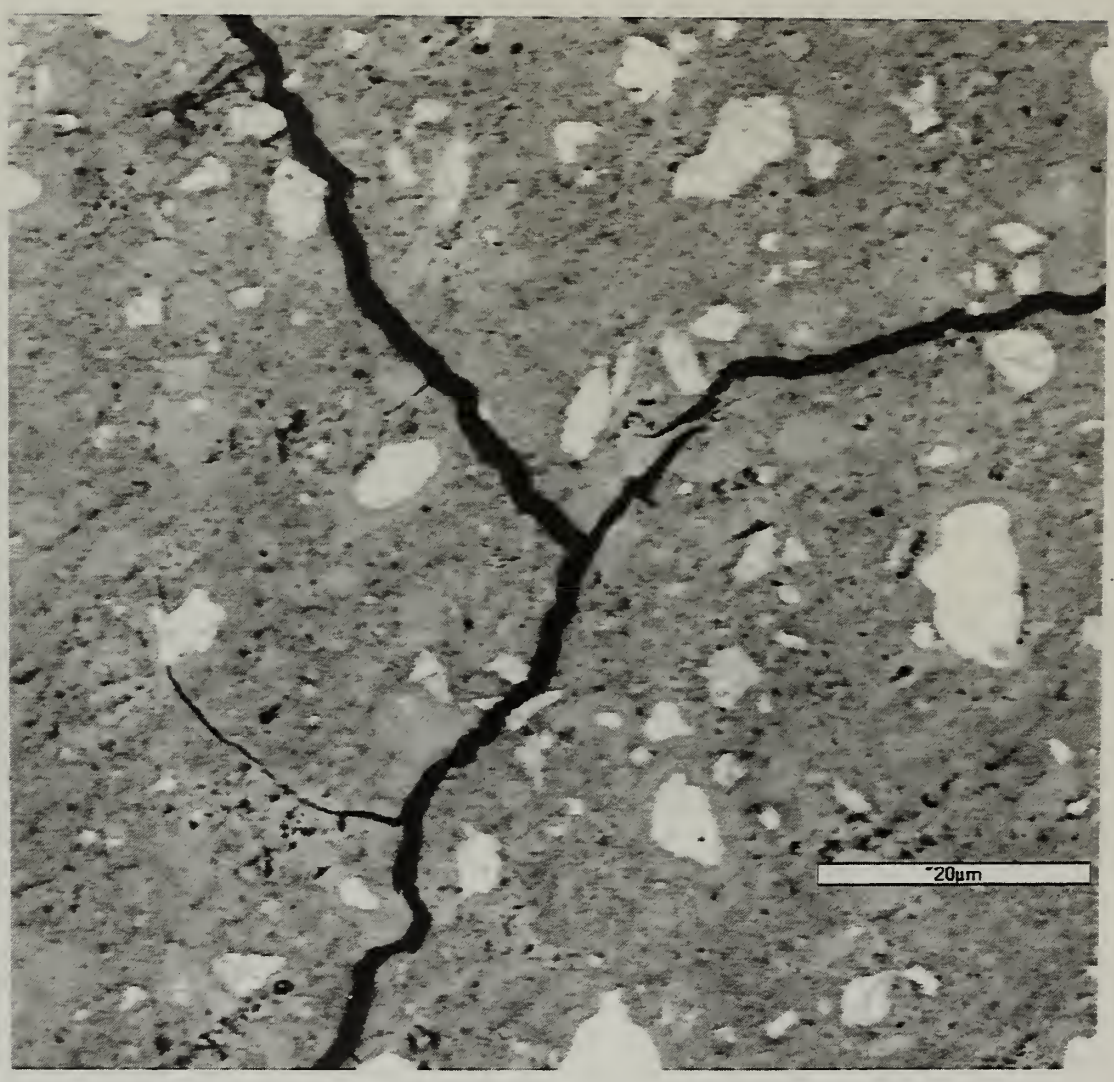


Figure 4.7 BSE SEM Micrograph of the as-received and hydrated powder sample.

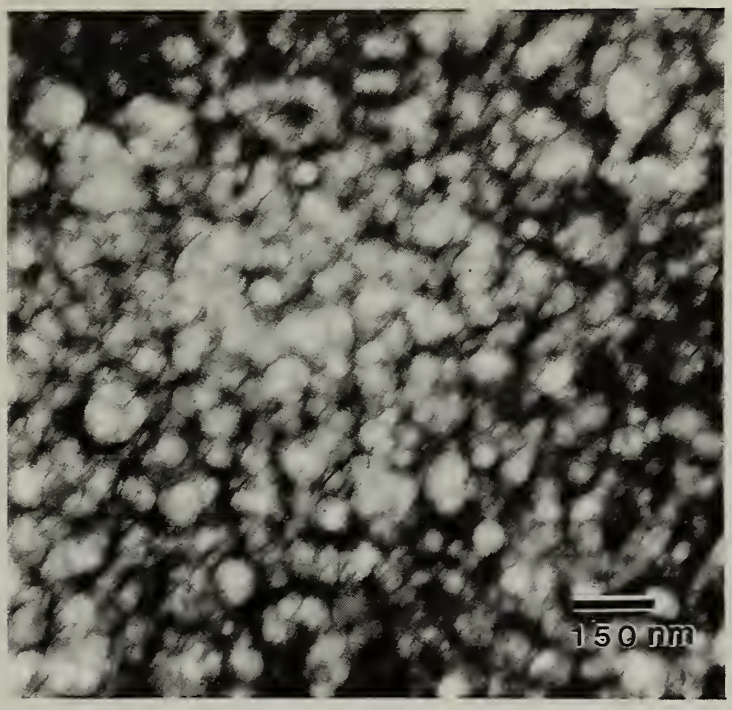


Figure 4.8 Bright-field TEM image of the C-S-H gel, showing the outer product area.

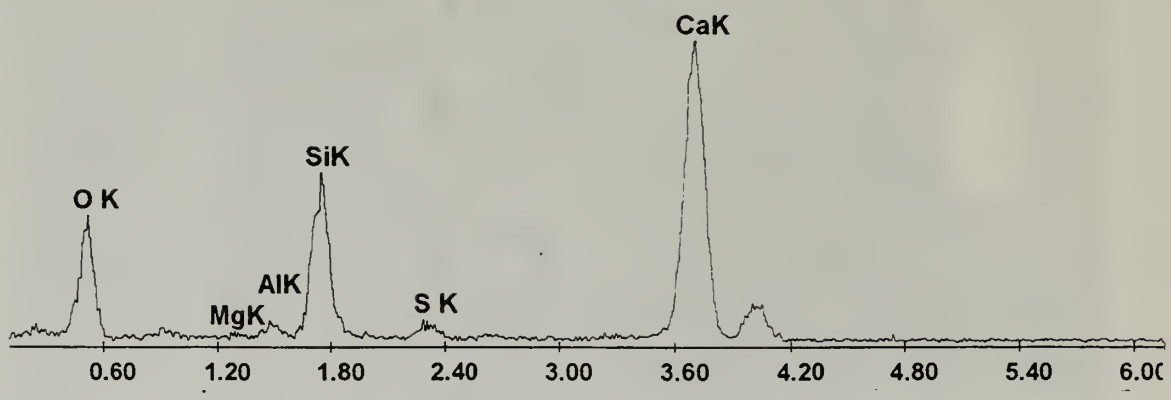


Figure 4.9 EDX spectra for the outer product C-S-H (shown in Figure 4.8) showing an average Ca:Si ratio of 1.76.

Figure 4.10 SAED pattern of the outer C-S-H gel region (shown in Figure 4.8) showing the presence of nanocrystallites regions coexisting with the C-S-H phase.

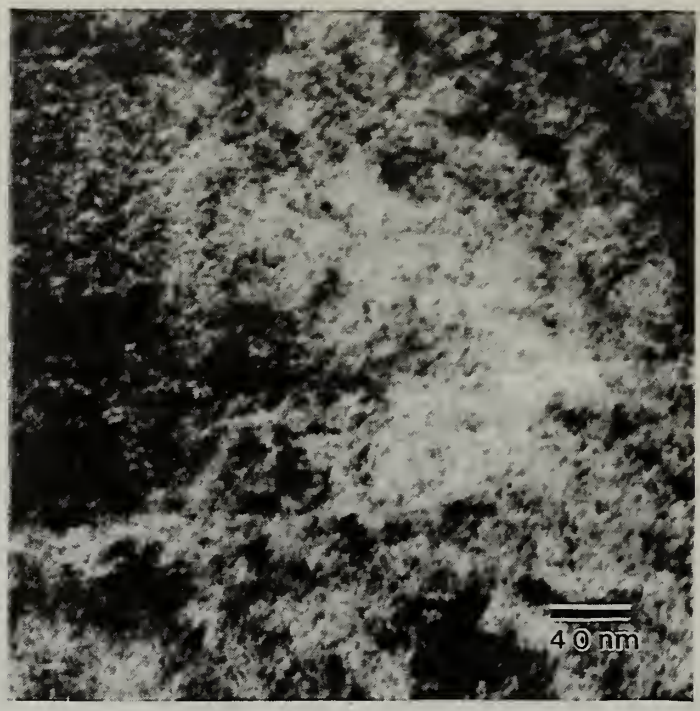


Figure 4.11 Bright-field TEM image of the inner product region of the C-S-H gel.

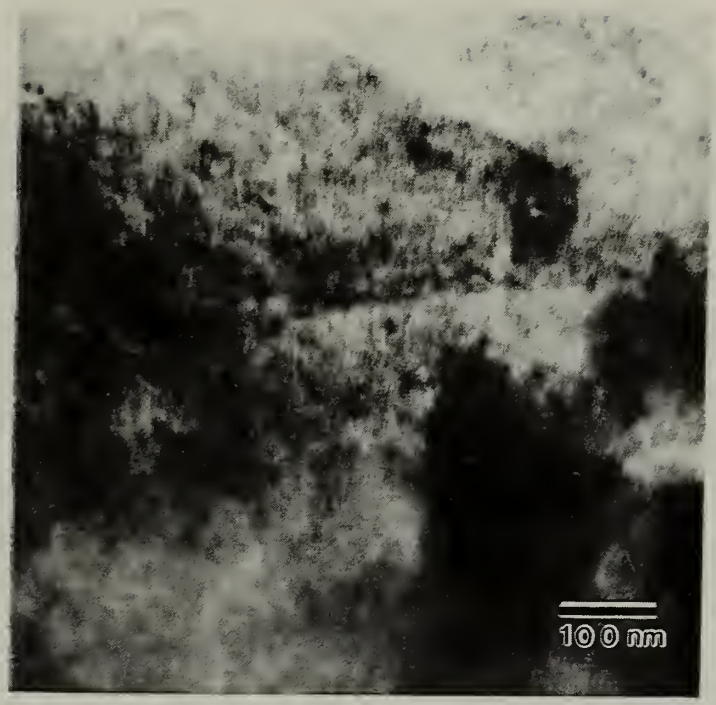


Figure 4.12 Bright-field TEM image taken from an inner/outer product interface region of the C-S-H gel.

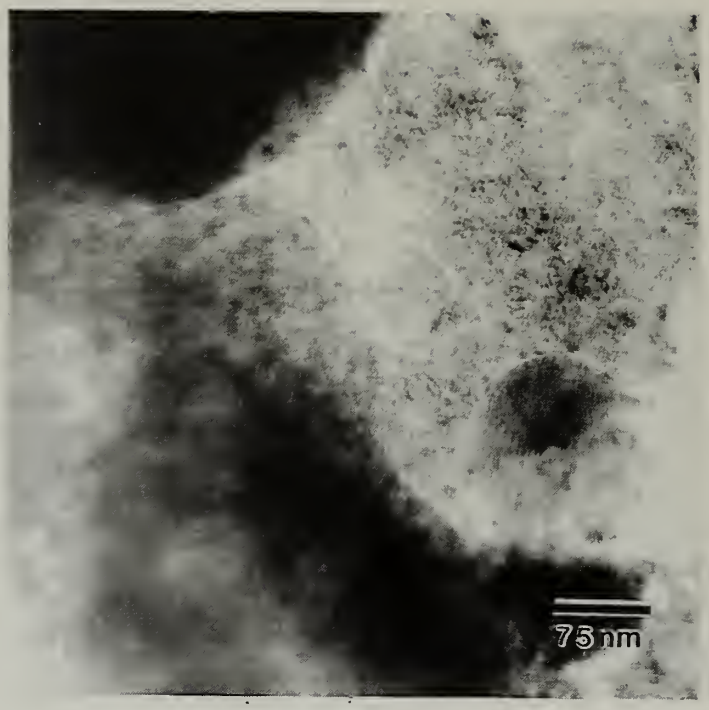


Figure 4.13 Bright-field TEM image taken at higher magnification for the inner/outer interface region shown in Figure 4.12.

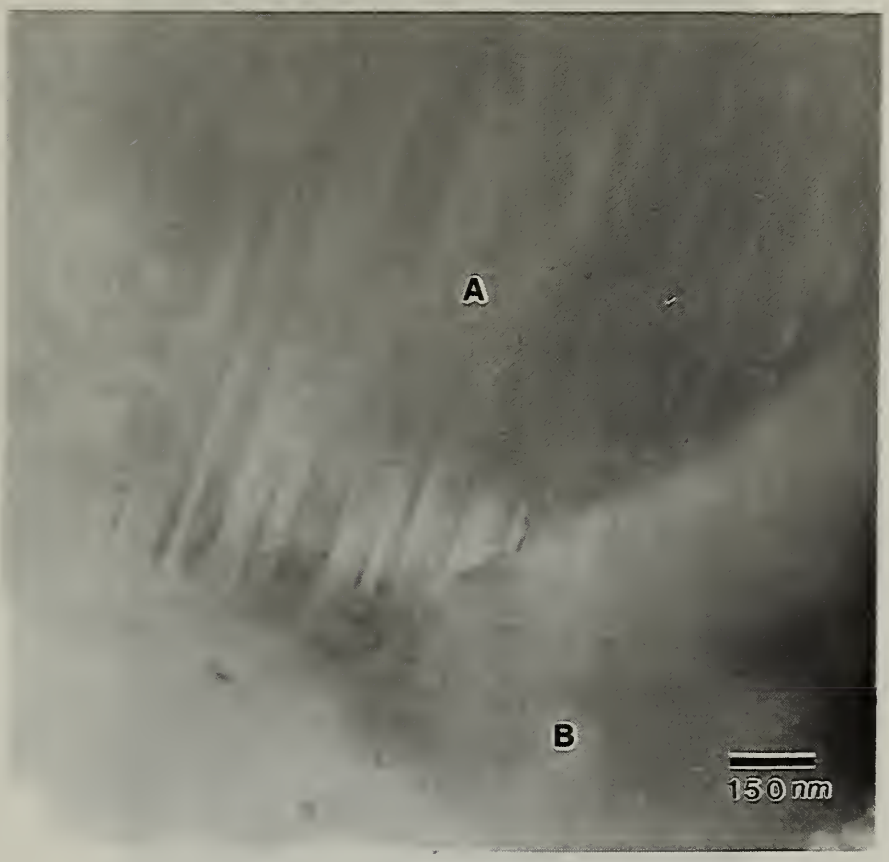


Figure 4.14 Bright-field TEM image showing unhydrated β-$C_2S$ with preexisting twins and C-S-H.

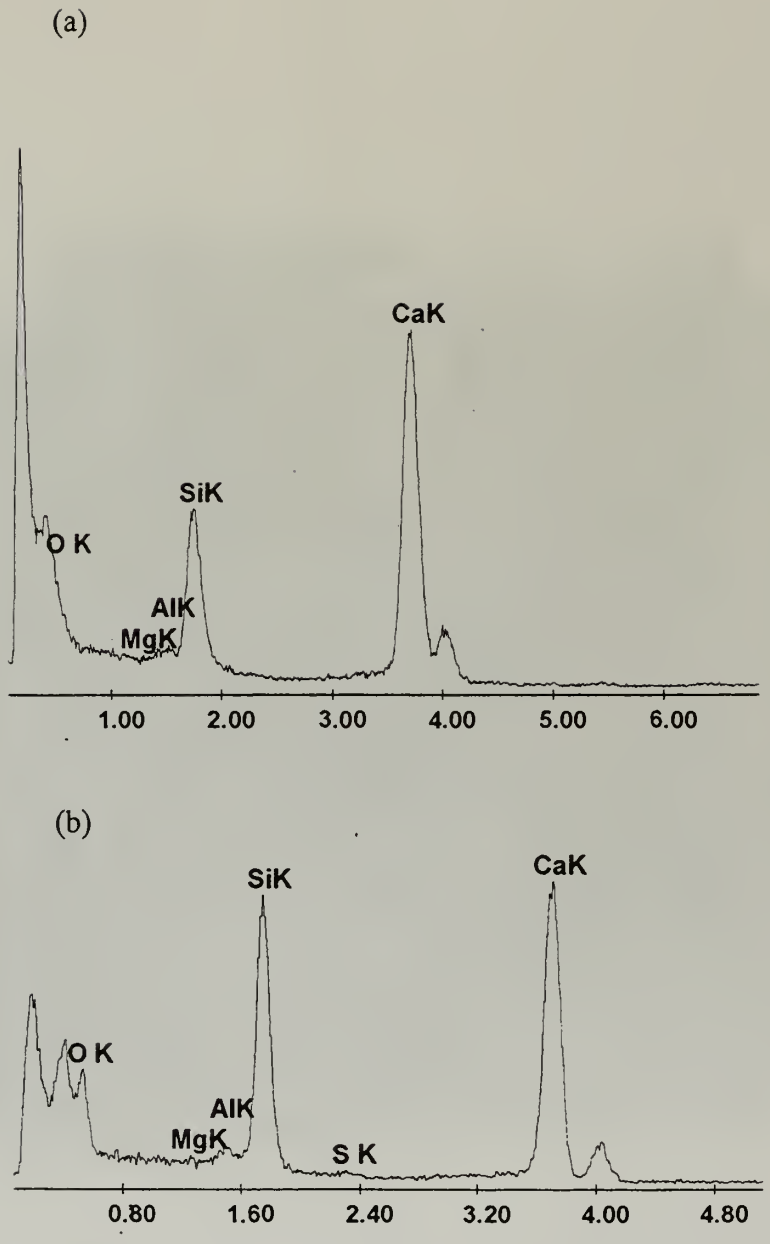


Figure 4.15 (a) EDX spectra for the unhydrated β-$C_2S$ and (b) EDX spectra for the C-S-H phase (shown in Figure 4.14).

(a)

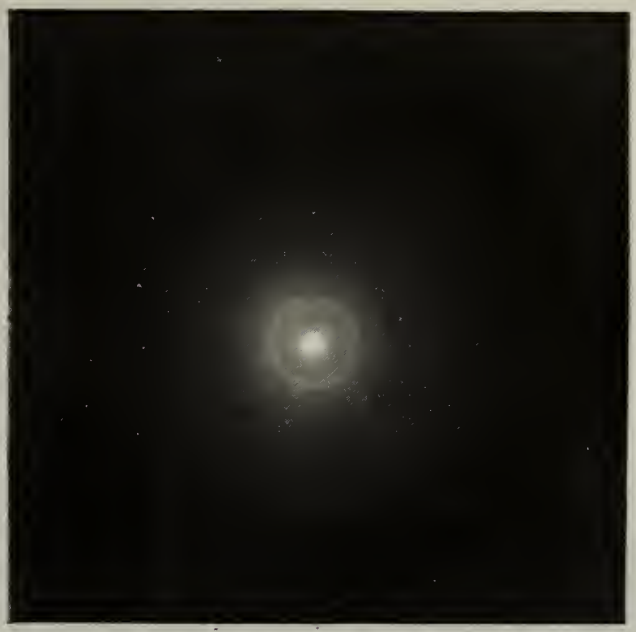

(b)

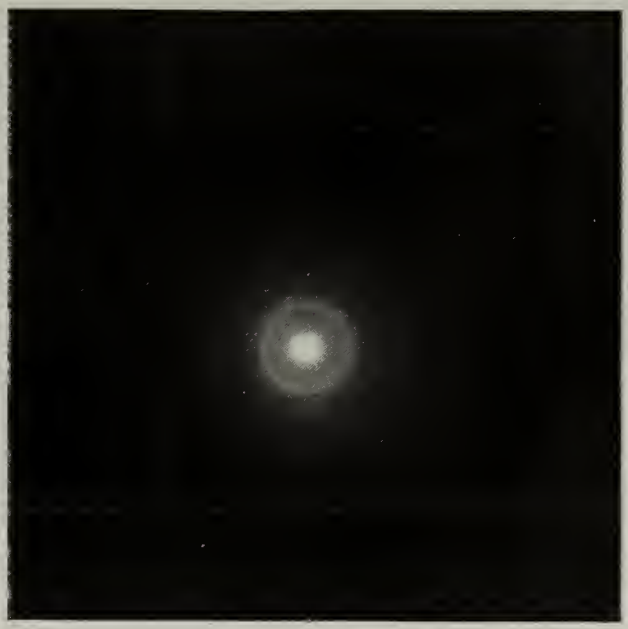

Figure 4.16 SAED patterns taken from various randomly selected regions within the C-S-H gel. The patterns clearly indicate the presence of diffuse rings.

Figure 4.17 SAED pattern taken from a randomly selected region within the C-S-H gel. The pattern clearly indicates the presence of diffuse rings.

Figure 4.18 Bright-field TEM image showing the presence of CH and C-S-H gel particles.

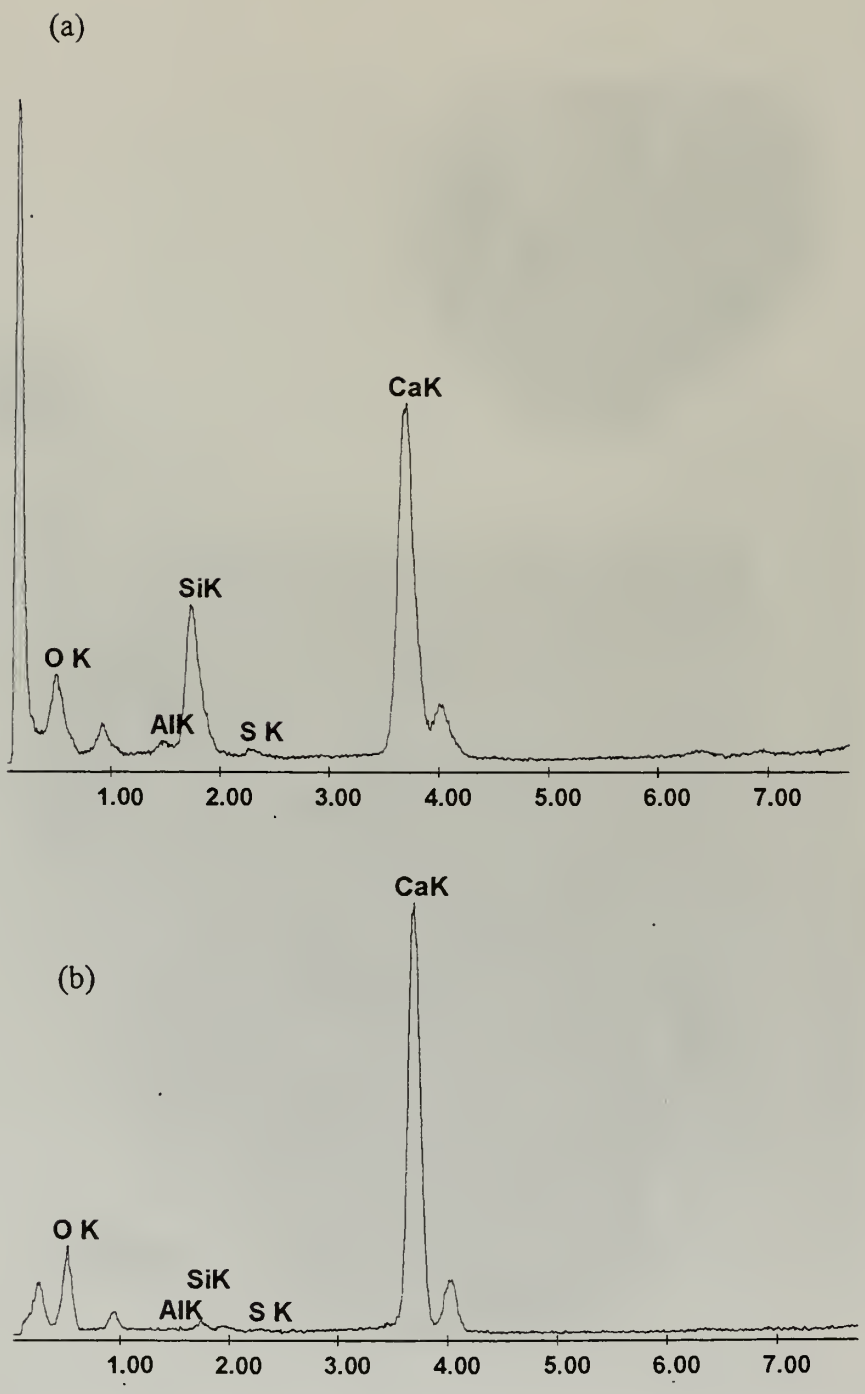


Figure 4.19 (a) EDX analysis of the C-S-H region, and (b) EDX analysis of the CH phase (shown in Figure 4.18).

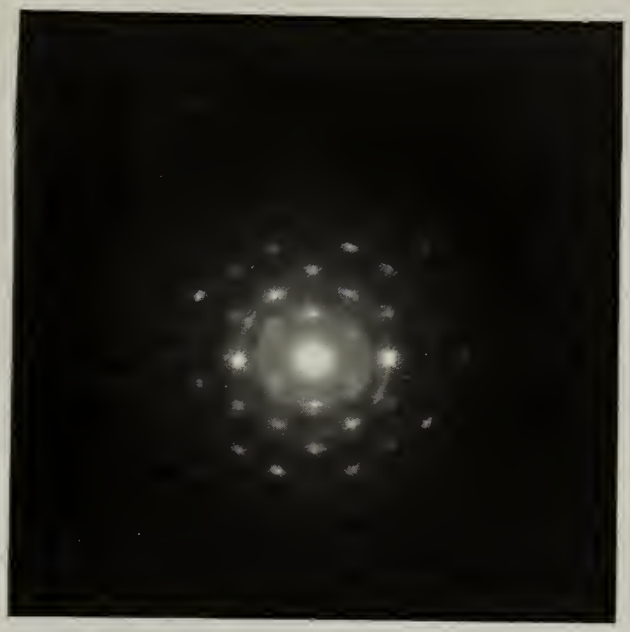

Figure 4.20 SAED for the CH region (shown in Figure 4.18). The electron beam direction is [110].

# V. SUMMARY

## A. CONCLUSIONS

The results of this study on the morphology and crystallography of a fully hardened Aalbrog Lion Brand Danish white cement paste with a w/c ratio of 0.25 indicate the following:

- The major crystallographic phases in the cement can be identified. These are:
  1. Unreacted $C_2S$.
  2. Unreacted $C_3S$.
  3. Portlandite CH ($Ca(OH)_2$).
  4. Small amounts of ettringite $Ca_6Al_2(SO_4,SiO_4,CO_3)_3(OH)_{12}.26H_2O$.
  5. Amorphous-like C-S-H (with some crystalline regions).

- The loss on ignition results indicate that the overall composition of the hydrated material is approximately $Ca_{1.75}.SiO_2.3H_2O$ and $Ca(OH)_2$ in equimolar amounts.

- SEM observations identified white equiaxed particles with sizes of approximately 10 μm (unreacted $C_3S$) and two hydrated regions. The light grey regions were described as inner product C-S-H gel and CH, and the dark grey regions were identify as outer product C-S-H gel and CH together with

other minor phases, such as ettringite. In addition, the dark grey region contained a great deal of porosity and other impurities.

- TEM observations of the C-S-H gel phases of the hardened cement revealed the presence of large Ca:Si ratio fluctuations with ranges between 0.35 to 5.74. In addition, short-range structural ordering and crystallinity (the presence of $Ca(OH)_2$ and $C_2S$) were demonstrated at the nanometer scale. In addition, the two hydrated regions (inner and outer product C-S-H) were found to differ in morphology. The inner C-S-H has a compact and homogeneous morphology and the outer C-S-H has a "honeycomb-like" morphology. The interfaces between the two hydrated regions were in general, poorly defined and thus difficult to characterize.

## B. RECOMMENDATIONS

There are further questions about the Aalbrog Lion Brand Danish white cement paste which may be addressed by transmission electron microscopy (TEM). The variation of C-S-H composition (in terms of both their chemical nature and microstructural development) with age may be verified by TEM studies after various time periods. This may provide insight leading to techniques for controlling microstructural development.

During the literature review it was apparent that researchers are currently looking at digital image processing that can be used in conjunction with scanning electron microscopy to investigate the microstructure of hydrated cements to provide quantitative

descriptions of the characteristics of the particles or other features present. This would provide interactive chemical image analysis of separable features in the backscattered images in the SEM.

Since many difficulties are encountered in quantitative X-ray diffraction analysis of portland cement, the next logical step is to obtain diffraction patterns by the use of neutron diffraction. It is recommended that future studies be conducted on the hydrated cement using a source of neutrons, such as a high flux reactor. The high penetration of neutrons allows studies to takes place on large volumes of sample getting away from the relatively small samples used for laboratory studies and getting closer to the real life situation.

It is also recommended that future studies be conducted on the microstructural features of Aalbrog Lion Brand Danish white cement with w/c ratios of 0.4 and 0.5. This would provide the basic information necessary to begin a trade-off analysis to ascertain the effects of water content in the mechanical properties.

## LIST OF REFERENCES


1. Sabine, T. M., Bertram, W. and Aldridge, L. P., "Microstructure of Hydrating Cement Paste", Australian Nuclear Science and Technology Organisation, Menai 2234, Australia, 1995.

2. Clark, S. M. and Barnes, P., "A comparison of laboratory, Synchrotron and Neutron Diffraction for the real time study of cement hydration", *Cement and Concreate Research*, v. 25, 1995.

3. Sabin, L. C., *Cement and Concrete,* Mcgraw Publishing Company, 1907.

4. Insley, H. and Frechette, V. D., *Microscopy of Ceramics and cements,* Academic Press Inc., New York, 1955.

5. Somerville, G., "Cement and concrete as materials: changes in properties, production and performance", *Proc. Instn. Civ. Engrs Structs and Blgs,* 1996.

6. Callister W. D., *Materials Science and Engineering: an Introduction,* John Wiley and Sons, 1994.

7. Van Vlack, L. H., *Physical Ceramics for Engineers,* Addison-Wesley Publishing, Inc., 1964.

8. Taylor, H. F. W., *The Chemistry of Cement*; Academic Press, London, U.K., 1992.

9. Viehland, D., Li, J. F., Yuan, L. J. and Xu, Z., "Mesostructure of Calcium Silicate Hydrate (C-S-H) gels in Portland Cement Paste: Short-Range Ordering, nanocrystallinity, and local composition order", *J.Am. Ceram. Soc.*, v. 79, 1996.

10. Richardson, I. G. and Groves, G. W., "Microstructure and microanalysis of hardened ordinary Portland cement pastes", *Journal of Material Science*, v. 28, 1993.

11. Meredith, P. and Donald, M., "Pre-induction and induction of tricalcium silicate: an environmental scanning electron microscopy study", *Chapman & hall,* 1995.

12. Diamond, S. and Bonen, D., "Microstructure of hardened Cement Paste a new interpretation", *J. Am. Ceram. Soc.*, v. 76, 1993.

13. Ma, W. and Brown, P. W., "Effect of phosphate additions on the hydration of Portland cement", *Advances in Cement research,* v. 6, 1994.

14. Richerson, D. W., *Modern Ceramic Engineering,* Marcel Dekker, Inc., New York 1992.

15. Uchikawa, H. and Hanehara, S., "Advances in the Characterization of Cement Clinker", Cement and Concrete research laboratory, Onada Cement Co., Ltd., Tokyo, Japan.

16. Diamond, S., "Interactive digital image feature analysis as applied to cement and concrete microstructural investigations", Proceedings of the Conference on Digital Image: Technique and Applications in Civil Engineering, Kona, Hawaii, USA.

17. Taylor, J. C. and Aldridge, L. P., "Full-profile Rietveld quantitative XRD analysis of Portland cement: Standard XRD profile for the major phase tricalcium silicate ($C_3S$: $3CaO.SiO_2$)", *Journal of Powder Diffraction*, v. 8, 1993.

18. Struble, L. J., "Quantitative Phase Analysis of Clinker Using X-Ray Diffraction", *Cement, Concrete, and aggregates*, CCAGDP, v. 13, 1991.

19. Senbetta, E. and Dolch, W. L., "The effect on cement paste of treatment with an extended set control admixture", *Cement and Concrete Research*, v. 21, 1991.

20. Mansoutre, S. and Lequeux, N., "Quantitative phase analysis of Portland cements from reactive powder concretes by X-ray powder diffraction", *Advances in Cement Research*, v. 8, 1996.

21. Saad, M., Abo-El-Enein, S. A., Hanna, G. B. and Kotkata, M. F., "Effect of Temperature on Physical and Mechanical Properties of Concrete containing Silica Fume", *Cement and Concrete Research*, v. 26, 1996.

22. Golovastikov, N. I., Matveeva, R. G. and Belov, N. V., "Crystal structure of the tricalcium silicate $3CaO.SiO_2 = C_3S$", *American Institute of Physics*, v. 20, 1976.

23. Sharma, M. and Harchand, K. S., "Mossbauer and x-ray diffraction studies of two dry and hydrated Portland cements and their clinker", *Cement and Concrete Research*, v. 21, 1991.

24. Mehta, S., Jones, R. and Caveny, B., "Cryogenics with cement microscopy redefines cement behavior", *Oil & Gas Journal*, Oct. 3, 1994.

25. Stutzman, P., "Cement and Concrete Characterization by Scanning Electron Microscopy", *Cement, Concrete, and* Aggregates, CCAGDP, V. 13, 1991.

26. Lange, D. A., Sujata, K. and Jennings, H. M., "Observations of wet cement using electron microscopy", *Ultramicroscopy*, v. 37, 1991.

27. Olek, J. and Diamond, S., "Alteration of polished sections of free lime containing cement clinker by short-term atmospheric exposure", *Cement and Concrete Research*, v. 21, 1991.

28. Senbetta, E. and Dolch, W. L., "The effects on cement paste of treatment with an extended set control admixture", *Cement and Concrete Research*, v. 21, 1991.

29. Fu, Y., Sheikh, S. A. and Hooton, R. D., "Microstructure of Highly Expansive Cement Pastes", *ACI Materials Journal*, v. 91, 1994.

30. Philippi, P. C., Yunes, P. R., Fernandes, C. P. and Magnani, F. S., "The Microstructure of Porous Building Materials: Study of a Cement and Lime Mortar", *Transport in Porous Media*, 1994.

31. Dimac, S. and Tepehan, F., "The effect of the inner structure on the absorptance of cement based exterior coatings", *Solar energy Materials and Solar Cells*, v. 33, 1994.

## INITIAL DISTRIBUTION LIST

No. Copies

1. Defense Technical Information Center
   8725 John J. Kingman Road, Ste 0944
   Ft. Belvoir, Virginia 22060-6218 ..... 2

2. Dudley Knox Library
   Naval Postgraduate School
   411 Dyer Rd.
   Monterey, California 93943-5101.. ..... 2

3. Naval/Mechanical Engineering Curricular Office, Code 34
   Naval Postgraduate School
   Monterey, California 93943-5000..... 1

4. Department Chairman, Code ME
   Department of Mechanical Engineering
   Naval Postgraduate School
   Monterey, California 93943-5000..... 1

5. Dr. Alan G. Fox, Code ME/FX
   Department of Mechanical Engineering
   Naval Postgraduate School
   Monterey, California 93943-5000..... 2

6. Dr. T. M. Sabine
   Australian Nuclear Science and
   Technology Organisation
   New Illawarra Rd., Lucas Heights NSW 2234
   PMB 1 Menai NSW. 2234..... 1

7. LT Fernando Maldonado
   Class 151
   Surface Warfare Officers School Command
   446 Cushing Road
   Newport, RI 02841-1209..... 3

DUDLEY KNOX LIBRARY
NAVAL POSTGRADUATE SCHOOL
MONTEREY CA 93943-5101

DUDLEY KNOX LIBRARY
3 2768 00341095 2